

Hyperfine interactions at dangling bonds in amorphous germaniumT. Graf,^{1,*} T. Ishikawa,² K. M. Itoh,^{2,3} E. E. Haller,⁴ M. Stutzmann,¹ and M. S. Brandt¹¹Walter Schottky Institut, Technische Universität München, 85748 Garching, Germany²Department of Applied Physics, Keio University, Yokohama 223-8522, Japan³JST-CREST, Kawaguchi, 332-0012, Japan⁴Department of Materials Science and Engineering, University of California, Berkeley, California 94720, USA

(Received 28 June 2003; published 20 November 2003)

Isotope-engineered amorphous germanium (*a*-Ge) films with ⁷³Ge concentrations in the range of 0.1 to 95.6% have been investigated by electron spin resonance (ESR) and electrically detected magnetic resonance (EDMR) at microwave frequencies between 0.434 and 9.35 GHz. The hyperfine interactions of dangling bond (DB) defects with many ⁷³Ge nuclei and their spin localization radius have been extracted from the broadening of the EDMR signals in isotope enriched samples at different ⁷³Ge concentrations. Linewidths as low as $\Delta B_{pp}^{\text{exp}} = 2.6$ G have been observed at 0.434 GHz in a sample without ⁷³Ge nuclear spins. At low ⁷³Ge concentrations, the frequency-dependent linewidth $B_{pp}^{\text{SO}}/\nu = 4.4$ G/GHz is determined by *g*-factor anisotropy and disorder. A frequency-independent linewidth contribution of about 1 G is attributed to dipolar broadening between the DB electronic spins. Over a large range of intermediate concentrations, the statistically distributed nuclear spins of ⁷³Ge atoms on sites close to the DB defect atom are responsible for the overall linewidth. The large linewidth $\Delta B_{pp}^{\text{exp}} = 300$ G of samples with ⁷³Ge concentrations of 95.6% requires a model wave function with a Fermi contact interaction of $A_{\text{iso}} = 29 \text{ G} \times g\mu_B$ at the defect atom, indicating that a fraction of 3.4% of the DB wave function originates from *s*-like orbitals there. The decay of the rest of the DB wave function can be described with a spin localization radius of 3.5 Å by a numerical model for the statistical hyperfine broadening. The delocalization of the DB spin is much smaller than that of the DB charge density determined in transport measurements.

DOI: 10.1103/PhysRevB.68.205208

PACS number(s): 71.23.Cq, 71.55.Jv, 76.30.Mi

I. INTRODUCTION

Dangling bonds (DB's) are the intrinsic defect states in group-IV semiconductors and were found to be responsible for both midgap acceptor and donor levels. Neutral DB's in Si have been studied in great detail, e.g., at the Si/SiO₂ interface¹⁻⁶ and in amorphous silicon (*a*-Si).⁷⁻¹³ In both cases, their electronic structure can be described as a linear combination of the valence orbitals of an undercoordinated central Si atom and of small contributions from the three backbonding hybrid orbitals. This was quantified experimentally via electron spin resonance (ESR) measurements of hyperfine interactions of the dangling bond electron spin with the nuclear spins $I_{29} = 1/2$ of the central and the backbonding ²⁹Si atoms. Owing to the technological importance of metal/oxide/semiconductor (MOS) field effect transistors based on crystalline Si, and of large area electronics such as displays and solar cells based on hydrogenated amorphous silicon (*a*-Si:H), DB's in Si have been comparatively well studied.

In particular for photovoltaic applications, amorphous alloys of Si with Ge are frequently used. After deposition, such films suffer from large concentrations of electrically active DB's in the range of $10^{18-20} \text{ cm}^{-3}$, which can be reduced by hydrogenation down to $10^{16-17} \text{ cm}^{-3}$.^{14,15} The resulting hydrogenated *a*-Si_{1-x}Ge_x:H films are then suitable for electronic applications. As shown experimentally by electrically detected magnetic resonance (EDMR),¹⁶ it is the Ge dangling bond that is responsible for most of the recombination processes also in Si-rich *a*-Si_{1-x}Ge_x:H alloys. This makes it important to understand DB's in *a*-Ge in detail. In

contrast to crystalline and amorphous Si, no detailed model for the structure of the defect orbital is available from measurements of the hyperfine interaction, for neither crystalline or amorphous germanium.

For both elemental semiconductors Si and Ge only one isotope exists with nonzero nuclear spin and at low natural abundance. The composition of natural Si is ²⁸Si (92.2%), ²⁹Si (4.7%), and ³⁰Si (3.1%). Natural Ge consists of ⁷⁰Ge (20.5%), ⁷²Ge (27.4%), ⁷³Ge (7.8%), ⁷⁴Ge (36.5%), and ⁷⁶Ge (7.8%). It can be expected that the hyperfine splitting of a dangling bond electronic spin is smaller for ⁷³Ge ($I_{73} = 9/2$) than that for ²⁹Si ($I_{29} = 1/2$), because the theoretical atomic hyperfine interactions from Hartree-Fock-Slater integrals at ⁷³Ge are about two times smaller than those at ²⁹Si,^{17,18} and because DB's in *a*-Ge are expected to be more delocalized than in *a*-Si.¹⁴ Unfortunately, the peak-to-peak linewidth $\Delta B_{pp}^{\text{exp}} = 48$ G observed for DB's in *a*-Ge at 9.35 GHz is much larger than $\Delta B_{pp}^{\text{exp}} = 8$ G for DB's in *a*-Si, so that the chances for the observation of resolved hyperfine satellites in *a*-Ge are rather low. The hyperfine contribution to the ESR linewidth of DB's in *a*-Ge was estimated in Ref. 19 from the method of moments^{20,21} to 17 G, assuming a localization radius of 5 Å. However, the authors suggested that these numbers should be verified using isotopically enriched samples.

In this work we investigate isotopically engineered amorphous Ge samples containing different concentrations of ⁷³Ge with the help of conventional ESR and EDMR at different microwave frequencies. We find a hyperfine broaden-

ing of 10 G at the natural isotope concentration, which is somewhat smaller than that predicted in Ref. 19, and determine the isotropic hyperfine interaction at the central defect atom to $29 \text{ G} \times g \mu_B$. From a numerical simulation of the EDMR linewidth over the complete ^{73}Ge concentration range, we are able to extract a spin localization radius of 3.5 Å for DB's in *a*-Ge. After the description of the experimental details and the electrical properties of the investigated samples in Sec. II, the EDMR spectra observed are discussed in Sec. III for *a*-Ge films deposited from pure *a*- ^{70}Ge material, from Ge with the natural isotope composition, and from ^{73}Ge -enriched samples at microwave frequencies from 0.434–9.35 GHz. Analytical models and numerical simulations for the interpretation of the observed broadening are presented in Sec. IV and then discussed with respect to the properties of DB's in *a*-Si in Sec. V. Taking into account the similarity of DB's in crystalline and amorphous Si, the results presented below can also be used as a first estimate for the structure of DB's in Ge crystals or at the Ge/GeO₂ interface. In addition, this investigation is a case study of the effects of the ^{73}Ge nuclear spins on the electron spins of paramagnetic states, which are relevant for recent proposals for quantum computation applications.²²

II. EXPERIMENTAL DETAILS

The *a*-Ge films under investigation were deposited on glass substrates (Corning 7059) by electron-beam evaporation of natural Ge and of isotopically enriched ^{70}Ge and ^{73}Ge target crystals with ^{73}Ge concentrations of 0.1 and 95.6%, respectively. The preparation of these crystals is described in more detail in Ref. 23. For the *a*-Ge films with intermediate ^{73}Ge concentrations of 31 and 51%, the appropriate amounts of ^{70}Ge and ^{73}Ge were electron-beam melted in a single Be crucible before deposition in order to ensure a homogeneous mixing. The substrates were cooled down to 77 K for the deposition of amorphous Ge films with a thickness around 1 μm. For the samples with low ^{73}Ge concentration, the densities of DB's could be determined by conventional ESR and were in the range of $10^{18-19} \text{ cm}^{-3}$. Defect densities of the samples with higher ^{73}Ge concentrations were similar, based on conductivity and optical absorption measurements. EDMR measurements were performed in a conventional CW X-band ESR spectrometer (Bruker ESP-300, with a TE₁₀₂ cavity) operating at 9.35 GHz, in a splitting S-band resonator (Bruker Flexline) operating at 2.00 GHz using an HP 83640A microwave generator and a 1 W power amplifier as the microwave source, and in a home-built helical L-band resonator operating at 0.434 GHz using a YAESU UHF ham radio transceiver and a 100 W power amplifier as the rf source. Care was used to avoid artificial broadening of the EDMR signal by magnetic field modulation and the incident microwave power. Unless otherwise specified, the measurement temperature was adjusted to around 70 K. No temperature-dependent broadening was observed in EDMR up to 100 K consistent with ESR studies on *a*-Ge:H, which report lifetime broadening of DB's in *a*-Ge:H above 150 K.^{14,24} At temperatures below 40 K, the detection

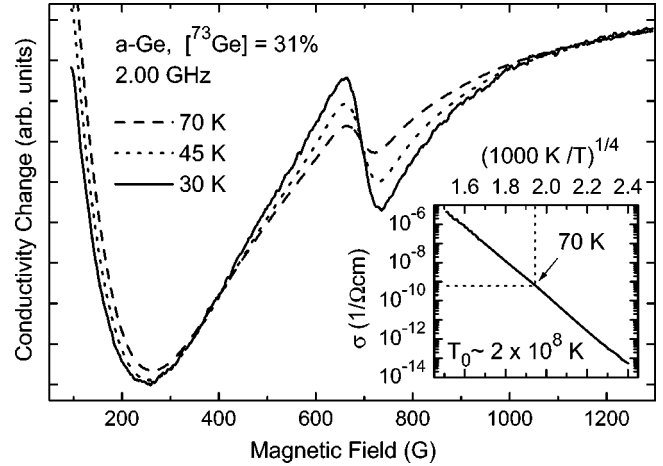


FIG. 1. Example for the temperature dependence of the EDMR signal normalized to the background caused by magnetoconductivity. The broad EDMR can be separated from the nonresonant background via its different temperature dependence. The inset shows the temperature dependence of the dc dark conductivity with the $\exp[(T/T_0)^{-1/4}]$ dependence typical for variable range hopping. The microscopic interpretation of T_0 in terms of the density of states and the localization radius is discussed in the context of Eq. (12).

of the EDMR signal is challenging because of the small sample conductivity.

For the electrical measurements, interdigitated Cr-Au contacts with finger spacings of 50 μm were deposited on $4 \times 10 \text{ mm}^2$ sample pieces. Because of substantial peeling off from the glass substrate during lithography, somewhat larger contacts had to be prepared manually with silver paint for one sample with $[^{73}\text{Ge}] = 31\%$. For the EDMR measurements, a dc voltage around 100 V was applied to the contacts, resulting in typical currents of the order of 1 μA at 70 K. Resonant current changes below 1 pA, which correspond to relative changes of the conductivity on a level of $\Delta\sigma/\sigma \approx 10^{-6}$, were resolved with good signal-to-noise ratio after amplification with a Stanford Research SR570 low-noise current preamplifier via magnetic field modulation, lock-in detection, and, in some cases, signal averaging for several days.

As shown previously for *a*-Si,²⁵⁻²⁷ the spin dependence of the hopping processes between adjacent DB's can be exploited for a very selective and sensitive detection of their ESR signal, which would be impossible otherwise for the films with high ^{73}Ge concentrations under investigation here. In addition, ESR spectra of thin film samples typically suffer from background impurities in the glass substrate and in other parts of the spectrometer. This is avoided in EDMR of *a*-Ge, as in measurements of spin-dependent dark conductivity only the resonant changes of paramagnetic states close to the Fermi level contribute. Typically, a nonresonant background is observed in EDMR because of the magnetic-field dependence of the conductivity. A possibility for the separation even of broad EDMR spectra from this magnetoconductivity background is shown in Fig. 1. While the EDMR intensity scales approximately as $\Delta\sigma \propto T$ in the investigated temperature range, the magnetoconductivity features were

found to scale rather similar to $\Delta m \propto T^2$. Therefore, the relative intensity $\Delta\sigma/\Delta m \propto T^{-1}$ is greatest at low temperatures, as shown in Fig. 1. In contrast to conventional ESR experiments, no quantitative information on the spin density can be extracted from the resonant changes in EDMR without the detailed knowledge of the relevant hopping rates. Therefore, the spectra shown below have been normalized to their peak-to-peak amplitude. Because of the high overall sample impedance, the best signal-to-noise and signal-to-background ratio is obtained at temperatures around 70 K.

The inset of Fig. 1 shows that the temperature-dependent dc conductivity falls off as $\sigma \propto \exp[(T/T_0)^{-1/4}]$, as expected for variable range hopping in unhydrogenated amorphous semiconductors with a large density of DB's close to the Fermi level.^{14,28,29} According to Ref. 30, the average tunneling range in such a material is proportional to $T^{1/4}$, since with increasing temperature a larger number of localized states is involved in the tunneling processes. To exclude significant exchange narrowing of the EDMR signals due to wave function overlap at large defect densities,³¹ we additionally investigated hydrogenated *a*-Ge:H films with natural isotope concentration, where the hopping rates are so small that no spin-dependent dark conductivity can be observed, because of the much lower defect density of the order of 10^{17} cm^{-3} . To perform EDMR on these samples, charge carriers were excited into the bands by illumination with white light or with the visible lines of a 5 W argon ion laser, and the spin-dependent effects on recombination were monitored through photoconductivity measurements.¹⁶ In contrast, no significant photoconductivity was observed in the unhydrogenated *a*-Ge films because of the higher defect density.

III. EXPERIMENTAL RESULTS

A. EDMR and ESR of pure *a*-⁷⁰Ge

The unhydrogenated *a*-⁷⁰Ge sample is virtually free from nuclear spins and therefore allows one to investigate the origin and magnitude of the contributions to the spin resonance linewidth other than hyperfine interaction. The remaining broadening mechanisms are dipolar and exchange broadening with neighboring DB's, lifetime broadening, as well as broadening by a distribution of *g* factors. The former mechanisms are expected to depend only weakly on the magnetic field, whereas the last mechanism is directly proportional to the field and to the microwave frequency (see Sec. IV A). As shown in Fig. 2, where the EDMR spectra are given as a function of the applied magnetic field *B*, the experimental linewidth for a pure *a*-⁷⁰Ge sample depends strongly on the employed microwave frequency and varies from only 2.6 G at 0.434 GHz to 43 G at 9.35 GHz. This indicates that it is mostly determined by *g*-factor broadening. Therefore, the same spectra are shown versus $g = h\nu/\mu_B B$ in Fig. 3, with Planck's constant *h*, Bohr's magneton μ_B , and the microwave frequency ν . Much closer similarity of the three spectra is indeed observed in this plot, as expected for *g*-factor broadening. However, also in Fig. 3 the linewidths and line shapes still do not coincide completely.

The dashed lines in Figs. 2 and 3 show a simultaneous curve fit assuming a distribution of *g* factors according to the

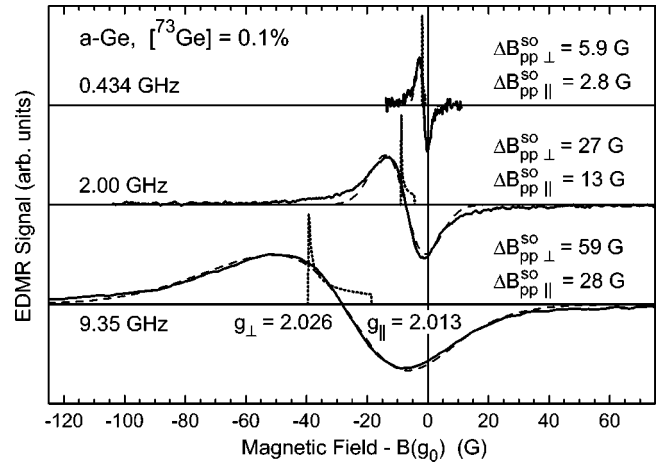


FIG. 2. EDMR signal of pure *a*-⁷⁰Ge at different microwave frequencies. The magnetic field axes are offset such that the fields corresponding to the resonance of free electrons with $g_0 = 2.0023$ coincide. The dashed lines are fits based on the powder patterns indicated by the dotted lines and on additional Gaussian broadening $\Delta B_{pp}^{SO}(\theta)$ because of disorder. $\Delta B_{pp}^{SO}(\theta)$ and $\theta = 0^\circ$ corresponds to DB's oriented parallel to the magnetic field direction, and $\Delta B_{pp}^{SO}(\theta)$ and $\theta = 90^\circ$ to DB's in perpendicular orientation.

same powder pattern for all spectra due to the random orientation of DB's in the amorphous network. This powder pattern is indicated by the dotted lines in Figs. 2 and 3 and is defined by the extremal *g* factors $g_\perp = 2.026$ and $g_\parallel = 2.013$ for the orientations of the external magnetic field parallel and perpendicular to the defect axis, i.e., the long axis of the dangling bond hybrid orbital.^{8,17} In addition, a Gaussian distribution of *g* factors needs to be considered for the simulation of the observed line shapes, similar to the fitting procedures of Refs. 7–9. Typically, the width $\Delta B_{pp}^{SO}(\theta)$ of such a distribution will depend on the orientation θ of the defect

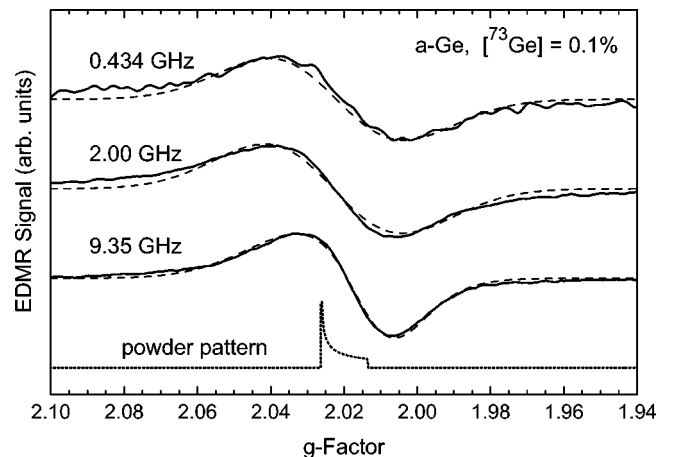


FIG. 3. Spectra and fits of Fig. 2, but now plotted versus a reverse *g*-factor axis. In the absence of nuclear spins, the linewidth is almost proportional to the microwave frequency, indicating that it is influenced dominantly by *g*-factor anisotropy. The smaller width at 9.35 GHz indicates a frequency-independent broadening mechanism, probably caused by dipolar electron-electron spin interactions of the order of 1 G at $N_S = 10^{19} \text{ cm}^{-3}$.

axis with respect to the external field. To reduce the number of possible fitting parameters $\Delta B_{pp}^{SO}(\theta)$ was assumed here to be proportional to the g -factor shift $g(\theta) - g_0$ from $g_0 = 2.0023$ of the free electron. Such a proportionality implies that the g -factor fluctuations causing the frequency-dependent broadening are caused by fluctuations of the spin-orbit interaction, which is also responsible for the g -factor shift with respect to the free electron value. The validity of this assumption is supported by the scaling of the linewidth $\Delta B_{pp}^{exp} = 8$ G of DB's in a -Si with the average g -factor shift $\bar{g} - g_0 = 3.2 \times 10^{-3}$ in comparison to DB's in a -Ge with $\Delta B_{pp}^{exp} = 48$ G and $\bar{g} - g_0 = 20 \times 10^{-3}$, which is proportional to the magnitudes of the spin-orbit coupling constants $\lambda_{Si} = 149 \text{ cm}^{-1}$ and $\lambda_{Ge} = 940 \text{ cm}^{-1}$.^{14,32} The average g factor $\bar{g} = 2.022$ of the powder patterns in Figs. 2 and 3 agrees with the reported values for $\bar{g} = \frac{1}{3}g_{||} + \frac{2}{3}g_{\perp}$, which were found in the range of 2.0018–2.023, and below 2.018 only in case of complex formation due to significant oxygen contamination.^{33–35} For DB's at the Ge/GeO₂ interface of crystalline germanium, $g_{\perp} = 2.022$ and $g_{||} = 2.005$ was reported in Ref. 36.

The width of the g -factor distributions visible in Fig. 3 (or the ratios of the linewidth and the corresponding microwave frequencies given in Fig. 2) seems to decrease at higher microwave frequencies, indicating a frequency-independent broadening mechanism of the order of 1 G. It can be estimated from the linewidths of the ⁷³Ge-enriched samples that such a broadening could only be accounted for by hyperfine interactions with ⁷³Ge, if the ⁷³Ge concentration in this nominally pure a -⁷⁰Ge sample was around 1%. This is not the case, as the residual ⁷³Ge concentration of the target crystal is only 0.1%, which suggests the presence of another frequency-independent broadening process in addition to the hyperfine interaction. Most probably, this process is the dipolar interaction between adjacent dangling bonds due to the high defect concentration in the investigated samples. An estimate for this dipolar broadening can be calculated based on the statistical theory of dipolar broadening (see Sec. IV B). For dipolar coupling between the electronic spins $S = 1/2$ of adjacent DB's, the calculation of Ref. 19 predicts a Lorentzian line with a linewidth

$$\Delta B_{pp}^{dip} = \frac{\pi}{9} \mu_0 \mu_B g N_S = N_S \times 0.82 \times 10^{-19} \text{ G cm}^3. \quad (1)$$

Dipolar broadening of the order of 1 G is indeed expected from this calculation for the spin density N_S of this a -⁷⁰Ge sample, which is about 10^{19} cm^{-3} . Therefore, dipolar electron electron spin interactions probably account for a significant fraction of the EDMR linewidth of the a -⁷⁰Ge films at 0.434 GHz. At X-band microwave frequencies, this contribution can be neglected for the analysis, because the observed linewidths are larger than 40 G. The effective dipolar distance would be reduced for an inhomogeneous distribution of DB's, so that Eq. (1) predicts a lower limit for the effective dipolar broadening. As the linewidth broadening observed is close to this limit, we can

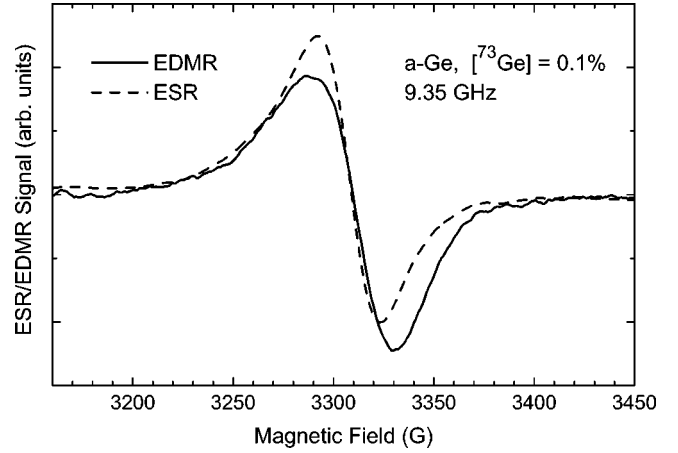


FIG. 4. Different line shapes of the ESR and EDMR signals of the same a -⁷⁰Ge sample under identical measurement conditions. A similar difference was observed in Ref. 16 for a -Ge:H with natural isotope concentration.

exclude strongly clustered DB's in our a -Ge films, unless exchange narrowing exactly compensates for the dipolar broadening (see Sec. III B).

A further peculiarity of EDMR of amorphous Ge, which was already reported earlier in Ref. 16 for a -Ge:H with natural isotopic composition, however without a detailed analysis, is found in the nuclear-spin free a -⁷⁰Ge-film in an even more pronounced way. As shown in Fig. 4, the ESR and EDMR spectra of the same a -⁷⁰Ge film show a very different line shape, although experimental conditions such as the applied microwave power, the modulation amplitude, and the speed of the magnetic field sweep were the same in both experiments. In particular, the EDMR line is somewhat broader and more asymmetric than the resonance line observed in conventional ESR. In contrast to the experiments of Ref. 16, in which spin-dependent photoconductivity was measured under illumination, lifetime broadening due to recombination does not play a role here, where the hopping conductivity of an a -⁷⁰Ge sample was monitored in the dark. The possible influence of the hopping processes on the linewidths will be found to be negligible in Sec. III B. It therefore appears likely that the main contribution to the spin-dependent dark conductivity comes from a particular subensemble of DB's in a -Ge, whereas all spins present in the sample, possibly also complexes of DB's with oxygen,³⁵ contribute equally to the microwave absorption in conventional ESR measurements. A subensemble of DB's dominating the EDMR signal could, e.g., be composed of those defects, which have a greater overlap than typical of their wave function with that of adjacent DB's. Consequently, the hopping rates will be increased at these DB's, which makes them more likely to participate in electronic transport, and the EDMR linewidth to be increased by dipolar interactions. Alternatively, a subensemble with increased coupling to neighboring spins could be characterized by relatively large g -factor fluctuations due to site-dependent fluctuations of the spin-orbit coupling. The hopping rate between such adjacent DB's is not high enough for the opposite effect on the linewidth to occur, a significant motional narrowing as observed

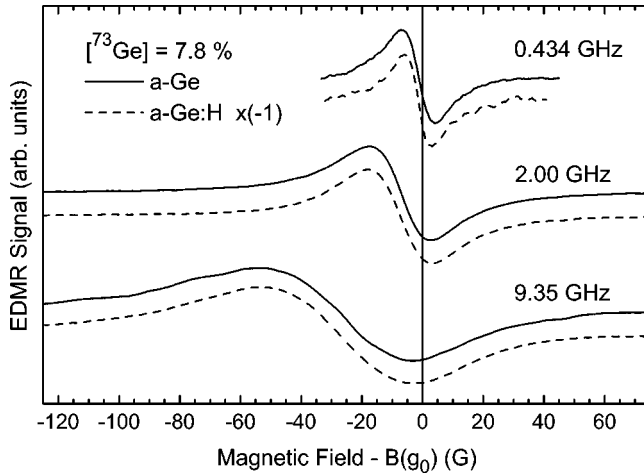


FIG. 5. EDMR signals of a -Ge with natural isotope concentration at different microwave frequencies. The magnetic field axes are offset such that the fields corresponding to $g_0=2.0023$ coincide. The dashed lines are spin-dependent photoconductivity measurements of hydrogenated a -Ge:H samples with significantly lower defect density. Under resonance conditions, the dark conductivity of a -Ge is enhanced, while the photoconductivity of a -Ge:H is quenched. For better comparison, the EDMR signals of a -Ge:H are therefore inverted. The larger linewidth of unhydrogenated a -Ge compared to a -Ge:H is probably caused by dipolar interactions between the electronic spins at 0.434 GHz.

in nearly metallic Si or SiC samples with similar concentrations of shallow donors.^{31,37} In the ^{73}Ge -enriched samples discussed below, the ESR background caused by defects in the substrate completely overwhelms the broad ESR signal of DB's in a -Ge, which is much weaker because of the hyperfine broadening taking place there. Since samples with similar densities of DB's of 10^{18} – 10^{19} cm^{-3} were used for the EDMR experiments studied here, the same subensemble of DB's participating in hopping transport will be relevant for the EDMR in the different films, independent of the nuclear spin concentration. The additional broadening of the EDMR resonance lines in these samples can therefore be attributed to hyperfine interactions.

B. EDMR of a -Ge and a -Ge:H with natural isotope composition

The EDMR linewidths observed for the sample free of ^{73}Ge nuclear spins now enable us to identify the additional broadening due to hyperfine interactions in ^{73}Ge -enriched samples. A comparison of Fig. 5 with the EDMR spectra of a -Ge with natural ^{73}Ge concentration $c=7.8\%$, and of Fig. 2 for pure a - ^{70}Ge shows that the EDMR lines of natural a -Ge broaden significantly at microwave frequencies of 0.434 and 2.00 GHz, while only a small broadening is caused by the ^{73}Ge nuclear spins at 9.35 GHz. The difference of the broadening effects is even more evident from a comparison of Figs. 6 and 3, where the spectra are shown versus the g factor. The linewidth at 0.434 GHz increases to 11 G by more than a factor of 4 in the sample with natural ^{73}Ge concentration compared to the nuclear-spin free

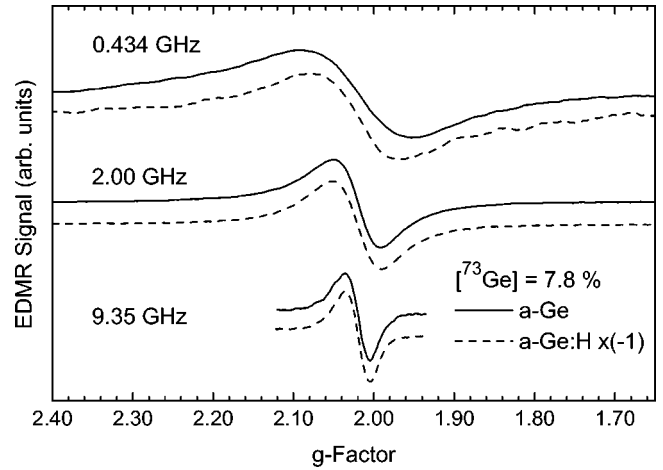


FIG. 6. The EDMR spectra of a -Ge with natural isotope concentration of Fig. 5 plotted versus a decreasing g -factor axis. Note the much wider g -factor scale in comparison to Fig. 3. The EDMR signals of a -Ge:H were again inverted for better comparison. Whereas the unresolved hyperfine broadening due to the nuclear spins is negligible at 9.35 GHz, it is significant at lower microwave frequencies.

a - ^{70}Ge sample. However, the probability $c/(1-c)$ to find DB's at a central ^{73}Ge nucleus is still below 10% for this nuclear spin concentration. Therefore, this broadening must originate from hyperfine interactions with a large number of surrounding nuclei.

To compare the effects of different spin-dependent processes and the total defect density on the EDMR signal, hydrogenated a -Ge:H samples of natural isotopic composition have been investigated. In Figs. 5 and 6, the spectra obtained via spin-dependent recombination in a -Ge:H are compared to the spectra obtained for spin-dependent hopping in a -Ge at the same ^{73}Ge concentration, but at a much lower density of DB's in the a -Ge:H sample. While an enhancement of spin-dependent hopping occurs in a -Ge under spin resonance conditions, a resonant quenching of the photoconductivity is observed in a -Ge:H.¹⁶ For better comparison, the EDMR spectra for a -Ge:H have been inverted in Figs. 5 and 6. For spin-dependent recombination at low defect concentrations, both the resonance of holes in the valence band tail, as well as a superposition of the resonances of DB's and electrons in the conduction band tail are observed in the spin-dependent photoconductivity of a -Si:H. However, at defect concentrations of 10^{17} cm^{-3} and above, the signal from DB's dominates in that material, as the spin-dependent hole diffusion process in the valence band tail is replaced by direct spin-independent tunneling of the hole to a doubly occupied dangling bond.³⁸ The same appears to be the case in our a -Ge:H films, where no indication of the valence band tail resonances with $g=2.054$ is found in spin-dependent recombination.¹⁴ The nearly identical EDMR resonances of a -Ge:H with $N_S \approx 10^{17}$ cm^{-3} and a -Ge with $N_S \approx 10^{19}$ cm^{-3} at 2.00 GHz and 9.35 GHz show that at this ^{73}Ge concentration, hyperfine and g -factor broadening are much stronger than the dipolar broadening of adjacent DB's, and that the effects of exchange interactions and the lifetime

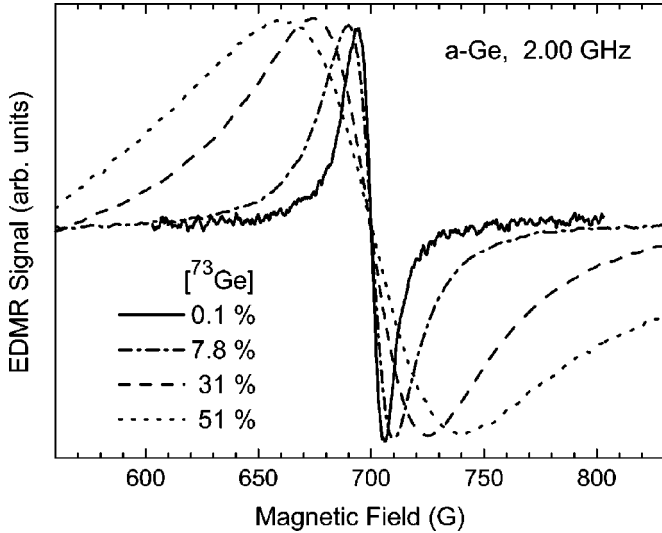


FIG. 7. Broadening of the EDMR spectra measured at 2.00 GHz of *a*-Ge depleted of ^{73}Ge , with natural ^{73}Ge concentration, and enriched with ^{73}Ge . The spectra are normalized for the same peak-to-peak amplitude and shifted to a common zero-crossing magnetic field.

dependence of hopping and recombination are negligible for the low-temperature linewidth.¹⁹ Only at the lowest microwave frequency of 0.434 GHz, the EDMR spectra of *a*-Ge:H and *a*-Ge differ significantly (see Fig. 6). The observed linewidth change is opposite to the hyperfine broadening expected from the nuclear spins of hydrogen in *a*-Ge:H, which is expected to be below 1 G, similar to the observations of Ref. 39 for *a*-Si:H. Therefore, the different low-frequency linewidths are most probably again related to the electron-electron spin dipolar broadening in the unhydrogenated *a*-Ge sample, to which the frequency-independent part of the EDMR linewidth of the *a*- ^{70}Ge sample was already attributed. Here, it is observed directly under the same experimental conditions as a linewidth difference in two samples with very different defect densities.

C. EDMR of ^{73}Ge -enriched samples

A further increase of the concentration c of ^{73}Ge nuclear spins does not lead to a resolved hyperfine structure in EDMR, as shown in Figs. 7 and 8. Instead, the spectrum broadens continuously to a linewidth of about 300 G at 9.35 GHz for the pure ^{73}Ge sample. This type of broadening is remarkable, as sudden increases of the linewidth or the development of substructure in the outer parts of some spectra would be expected for any characteristic hyperfine interaction. Because of the magnetoconductivity background and the large EDMR linewidth, no resonances were resolved for the *a*- ^{73}Ge sample with $c=95.6\%$, and for 0.434 GHz at $c \geq 31\%$. In addition to the EDMR linewidth, which varies over more than two orders of magnitude due to the variation of the concentration of nuclear spins, the line shapes are changing significantly from a close to Lorentzian shape at $c \leq 51\%$ to a Gaussian shape at $c = 95.6\%$. The arrow in Fig. 8 indicates the onset of a shoulder in the spectrum with c

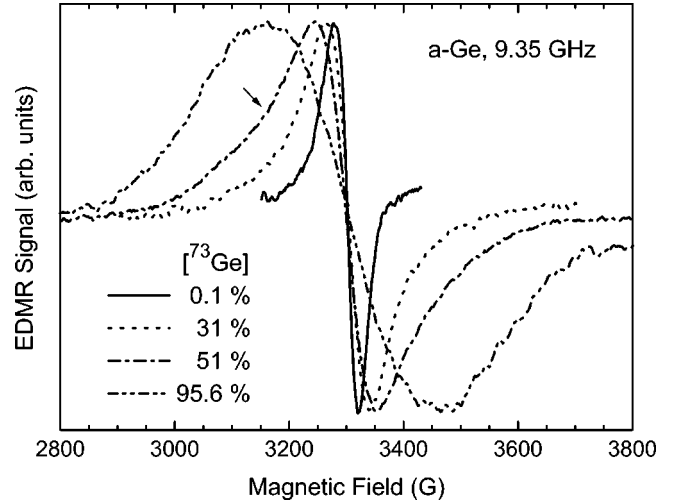


FIG. 8. EDMR spectra at 9.35 GHz for the complete range of ^{73}Ge concentrations. Note that the narrow spectrum with $c = 0.1\%$ is identical with the broadest spectrum of Fig. 2. The arrow indicates the onset of a shoulder in the spectrum with $c = 51\%$.

$= 51\%$, which is interpreted as a remainder of the unresolved central Fermi contact interaction in the following sections. A similar shoulder around $\pm(100-200)$ G from the center of the spectrum is weakly observed in the wings of the 2.00 GHz spectrum of the sample with $c = 51\%$. In this case, it overlaps less with the central line, but cannot be separated from the magnetoconductivity background unambiguously.

The peak-to-peak linewidths measured by EDMR in this work at different isotope concentrations and microwave frequencies are summarized in Table I. As discussed above, the linewidths increase significantly with the ^{73}Ge concentration. The largest change is observed at 9.35 GHz between $c = 51$ and 95.6% . The uncertainties of $\Delta B_{pp}^{\text{exp}}$ listed in Table I arise mostly from the possible errors during the subtraction of the magnetoconductivity background. Also included in Table I are the line shape factors obtained via double integration of the measured derivative EDMR spectra $y'(B)$ with the peak-to-peak amplitudes $\Delta y'_{pp}$

$$l = 2 \int \int y'(B) dB^2 / \Delta y'_{pp} \Delta B_{pp}^2. \quad (2)$$

For the double integration, a spectral range of at least $8 \times \Delta B_{pp}$ was employed for all values except for the line shape factors marked explicitly. The line shape factor defined by Eq. (2) is 1.033 for a Gaussian line and 3.628 for a Lorentzian line. Mostly Gaussian line shape factors are found for the spectra at 9.35 GHz and low ^{73}Ge concentrations, as these spectra can be understood to be caused by a powder pattern and a Gaussian distribution of g factors. At higher ^{73}Ge concentrations, the line shape factors increase towards the Lorentzian value at all microwave frequencies. Only the very broad EDMR spectrum at $c = 95.6\%$ shows a clear Gaussian line shape again. The reasons for this characteristic behavior will be discussed in detail in the following sections.

TABLE I. Observed peak-to-peak linewidths $\Delta B_{pp}^{\text{exp}}$ and line shape factors l for the derivative EDMR spectra of Figs. 2–8. The uncertainties of $\Delta B_{pp}^{\text{exp}}$ arise mostly from the possible errors due to the subtraction of the magnetoconductivity backgrounds. For the double integration, a spectral range of $8 \times \Delta B_{pp}^{\text{exp}}$ was employed for all lines except when a narrow integration range of $3 - 6 \times \Delta B_{pp}^{\text{exp}}$ is indicated by an asterisk. In these cases, the wings had to be estimated from the well resolved central part of the EDMR spectra.

	[^{73}Ge] (%)	Linewidth $\Delta B_{pp}^{\text{exp}}$ (G)			Line shape factor l		
		0.4 GHz	2 GHz	9 GHz	0.4 GHz	2 GHz	9 GHz
<i>a</i> -Ge	0.1	2.6 ± 0.2	12 ± 1	43 ± 2	2.4 ± 0.3	2.6 ± 0.3	1.6 ± 0.2
<i>a</i> -Ge	7.8	11 ± 1	21 ± 1	48 ± 2	2.2 ± 0.4	2.8 ± 0.2	2.1 ± 0.2
<i>a</i> -Ge:H	7.8	9 ± 1	21 ± 1	47 ± 2	2.8 ± 0.4	2.9 ± 0.3	2.2 ± 0.2
<i>a</i> -Ge	31		52 ± 3	73 ± 4	$3.0^* \pm 0.4$		2.6 ± 0.3
<i>a</i> -Ge	51		78 ± 5	112 ± 7	$3.3^* \pm 0.7$		3.0 ± 0.3
<i>a</i> -Ge	95.6			300 ± 10			$1.1^* \pm 0.2$

IV. HYPERFINE INTERACTIONS WITH ^{73}Ge

A. Spin Hamiltonian

The spin Hamiltonian of isolated, singly occupied dangling bonds is dominated by the Zeeman interaction given by the axial g -tensor \hat{g} and the external magnetic field \vec{B} . Additionally, the Hamiltonian contains all hyperfine interactions \hat{A}_n with the surrounding nuclear spins I_n

$$\mathcal{H} = \mu_B \vec{S} \hat{g} \vec{B} + \sum_n \vec{S} \hat{A}_n \vec{I}_n. \quad (3)$$

For axial hyperfine tensors with only small anisotropic components, the effective hyperfine interactions are given by $A_n = A_{n,\text{iso}} + A_{n,\text{aniso}}(3 \cos^2 \theta - 1)$ for orientations of the hyperfine axes at an angle θ with respect to the magnetic field. At the microwave frequencies used, the resonance fields for ESR transitions are given approximately by

$$B = \frac{h\nu}{g\mu_B} - \sum_n \frac{A_n}{g\mu_B} m_n - \sum_n \frac{A_n^2 [I(I+1) - m_n^2]}{2g\mu_B h\nu} + \dots, \quad (4)$$

where the magnetic quantum number takes the values $m_n = -I, \dots, +I$ for the ^{73}Ge nuclei with nonzero nuclear spin $I = 9/2$, and with $I = 0$ otherwise. The energy eigenvalues and the magnetic fields, at which the strongly allowed ESR transitions occur at $\nu = 0.434$ GHz and 2.00 GHz are shown in Fig. 9 for an isotropic Zeeman interaction with $g = 2.022$, i.e., for $h\nu/g\mu_B = 154$ and 707 G, and for an isotropic hyperfine interaction $A_{0,\text{iso}} = 29 \text{ G} \times g\mu_B$ with a single nuclear spin. To first-order perturbation theory, the transition fields are given by $2I+1$ equally spaced hyperfine satellites centered around the dominant Zeeman field. All transitions are shifted towards lower magnetic fields due to the second-order term of Eq. (4), which must be taken into account, e.g., for the $[\text{GeO}_4]^-$ center in α -quartz at X-band frequencies.⁴⁰ We will show below that hyperfine interactions as large as $29 \text{ G} \times g\mu_B$ are indeed present in *a*-Ge, but have significant influence on the linewidth only at $c > 60\%$. Since the EDMR spectrum of the sample with $c = 95.6\%$ could be separated clearly from the magnetoconductivity background only at $\nu = 9.35$ GHz, and since also the other hyperfine broadenings

listed in Table I do not exceed the respective resonant magnetic field by more than 12%, it is sufficient to restrict the linewidth analysis to the first-order terms of Eq. (4) only.

A purely isotropic hyperfine interaction A_{iso} as discussed above is characteristic for spin states with spherically symmetric (*s*-like) dangling bond wave functions. The simplest approach for a complete microscopic description of a dangling bond wave function Ψ_{db} involves the linear combination of the $4s$ and $4p$ valence orbitals Ψ_s and Ψ_p of the outer shell of Ge atoms at the atomic sites \vec{r}_n

$$\Psi_{db}(\vec{r}) = \sum_n \alpha_n \Psi_s(\vec{r} - \vec{r}_n) + \beta_n \Psi_{p_x, p_y, p_z}(\vec{r} - \vec{r}_n). \quad (5)$$

Neglecting the overlap of the different atomic orbitals within this superposition, and the core states and bonding orbitals such as the $3d$ states not included in this form of Ψ_{db} , a one-to-one correspondence between the hyperfine parameters

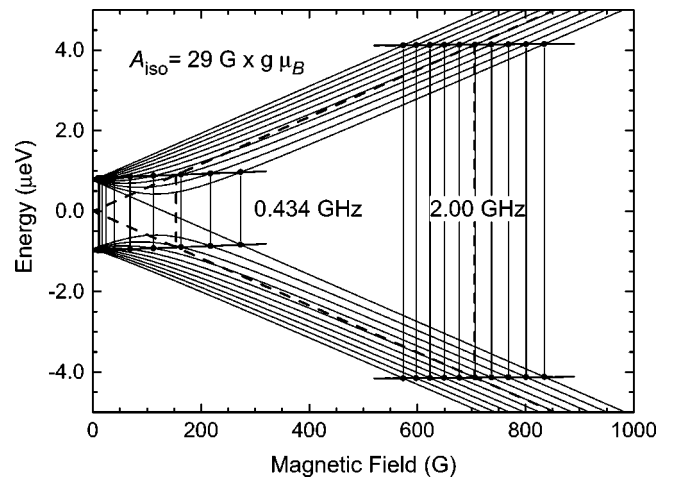


FIG. 9. Breit-Rabi diagram for the spin Hamiltonian (3) with a single isotropic g factor $g = 2.022$ and hyperfine interaction $A_{0,\text{iso}} = 29 \text{ G} \times g\mu_B$. The transition fields for electron spin resonance at 0.434 and 2.00 GHz are shown by the vertical lines. Indicated by the dashed lines are the energy levels and transition fields without perturbations by a nuclear magnetic moment.

$A_{n,\text{iso}}$ and $A_{n,\text{aniso}}$, and the projections α_n^2 and β_n^2 of the dangling bond wave function onto the atomic wave functions $\Psi_s(\vec{r}-\vec{r}_n)$ and $\Psi_p(\vec{r}-\vec{r}_n)$ is obtained for locally axial symmetry.^{8,17,18} The isotropic hyperfine parameters $A_{n,\text{iso}}$ are then interpreted as local Fermi contact interaction of the s -like components of the model wave function of Eq. (5). The anisotropic parameters $A_{n,\text{iso}}$ are interpreted as the local dipolar interaction of the p -like components of the electronic spin with the ^{73}Ge nucleus with index n , so that

$$A_{n,\text{iso}} = \alpha_n^2 A_{\Psi_s} = \alpha_n^2 \frac{2\mu_0}{3} g \mu_B g_n \mu_n |\Psi_s(0)|^2,$$

$$A_{n,\text{aniso}} = \beta_n^2 A_{\Psi_p} = \beta_n^2 \frac{2\mu_0}{5 \times 4\pi} g \mu_B g_n \mu_n \langle r^{-3} \rangle, \quad (6)$$

where $\mu_0 = 4\pi \times 10^{-7}$ Vs/Am, g_n and μ_n denote the nuclear g factor and the nuclear magneton, $|\Psi_s(0)|^2$ and $\langle r^{-3} \rangle$ are the characteristic atomic spin density and dipolar distance, and $n=0$ is used to label the central defect atom. Long-range dipolar broadening of electronic spins centered at the central defect atom with the nuclear spins of the surrounding ^{73}Ge nuclei can be estimated via the statistical theory in the point-dipole approximation, similar to Eq. (1). This broadening is found to be below 1 G and insignificant at all nuclear spin concentrations. The atomic hyperfine interactions $A_{\Psi_s} = 843 \text{ G} \times g_0 \mu_B$ and $A_{\Psi_p} = 17 \text{ G} \times g_0 \mu_B$ have been calculated using Hartree-Fock-Slater integrals,¹⁷ so that in principle the fractions α_n^2 and β_n^2 of the dangling bond wave function can be mapped out with the measured hyperfine parameters.

In $a\text{-Si:H}$, it was concluded that $\alpha_0^2 = 6\%$ of the electronic spin wave function comes from a $3s$ orbital at the central defect atom, and about $\beta_0^2 = 50\%$ from a nonbonding $3p$ orbital. About $\alpha_1^2 + \beta_1^2 \approx 10\% - 20\%$ of the spin wave function in $a\text{-Si:H}$ comes from at least one of the backbonding sp^3 hybrid orbitals.⁸⁻¹¹ Similar to ^{29}Si , which is the only Si isotope with nonzero nuclear spin $I_{29} = 1/2$, only ^{73}Ge with a natural abundance of 7.8% has a nonzero nuclear spin $I_{73} = 9/2$. The relative intensity of each of the $2I+1$ hyperfine satellites at a given nuclear spin concentration c in $a\text{-Ge}$ is expected to be $c/(2I_{73}+1) = c/10$, which is five times smaller than $c/(2I_{29}+1) = c/2$ in $a\text{-Si}$. In addition to this lower intensity, the smaller atomic hyperfine interactions of Ge compared to Si would lead to smaller hyperfine splittings in $a\text{-Ge}$,¹⁷ even if the wave functions would be the same in both materials. Even smaller hyperfine splittings can be expected from the larger delocalization of the dangling bond wave function in $a\text{-Ge}$ estimated from electrical measurements.¹⁴

In contrast to DB's in $a\text{-Si:H}$, no resolved satellite peaks are therefore observed for $a\text{-Ge}$ in Figs. 7 and 8. However, characteristic changes in the EDMR linewidth $\Delta B_{pp}^{\text{exp}}$ are found upon ^{73}Ge dilution and enrichment, as summarized in Fig. 10, where the experimental peak-to-peak linewidth is shown for all $a\text{-Ge}$ samples and resonance frequencies investigated. In a first approach, the large range of linewidths can be understood empirically by a convolution of three contri-

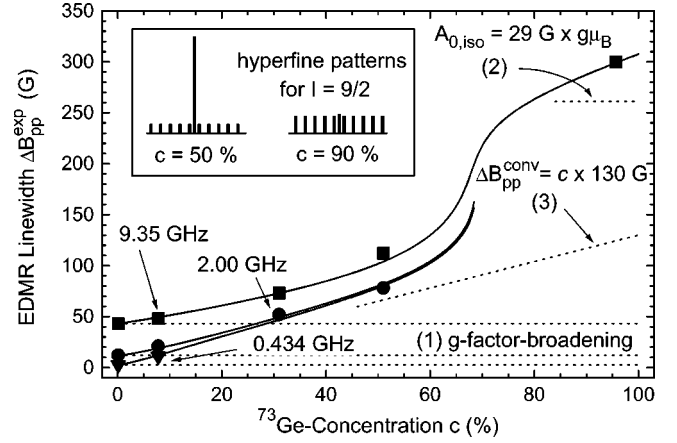


FIG. 10. Experimentally determined peak-to-peak linewidths $\Delta B_{pp}^{\text{exp}}$ of the spectra shown in Figs. 2–8. The continuous lines were calculated from a convolution assuming (1) a frequency-dependent Gaussian broadening due to a g -factor distribution, (2) a central hyperfine interaction of $29 \text{ G} \times g \mu_B$, which itself would lead to a spread of hyperfine satellites over 261 G, and (3) a Lorentzian broadening $\Delta B_{pp}^{\text{conv}}$ due to the surrounding spins, which increases linearly with the nuclear spin concentration c . The intensity patterns for $c=50$ and 90% shown in the inset explain the qualitative change around $c=70\%$ due to contribution (2), which causes the sudden increase of the linewidth by more than 100 G.

butions, which are indicated by the dotted lines in Fig. 10. The first contribution is an approximately Gaussian g -factor broadening independent of the ^{73}Ge concentration, but dependent on the employed microwave frequency. This contribution is known explicitly from the nuclear-spin free $a\text{-}^{70}\text{Ge}$ film discussed in Sec. III A. Secondly, a hyperfine pattern is taken into account, which is caused by a single isotropic hyperfine constant $A_{\text{iso}} = 29 \text{ G} \times g \mu_B$ arising from the Fermi contact interaction with the central defect atom. As shown by the inset in Fig. 10, the intensity of the hyperfine satellites of a single ^{73}Ge nucleus is rather small at $c \leq 50\%$ and comparable to the intensity of the central line only at $c \geq 90\%$, so that this contribution can be extracted best from the linewidth of the sample with $c = 95.6\%$. The third, at this point empirical component is a Lorentzian line whose peak-to-peak linewidth $\Delta B_{pp}^{\text{conv}} = c \times 130 \text{ G}$ varies linearly with the ^{73}Ge concentration c . This component is important for the increase of the linewidth from $c = 7.8$ to 51%. The resulting linewidths from the convolution of these three contributions are included as solid lines for the different measurement frequencies in Fig. 10. One of the most characteristic features of this calculation is the slow increase of the linewidths at low nuclear spin concentrations, and the sudden increase by more than 100 G around $c = 70\%$. As indicated by the inset of Fig. 10, this feature is not unexpected, and based on the intensity ratios of the hyperfine patterns of a single ^{73}Ge nucleus. The central resonance dominates the experimentally observed linewidth $\Delta B_{pp}^{\text{exp}}$ at ^{73}Ge concentrations below 70%, and the much broader envelope of the hyperfine satellites above. The only free parameters in such a convolution are the magnitude of the central hyperfine interaction, and the slope $\Delta B_{pp}^{\text{conv}}/c$ of the linearly

increasing broadening component, which can be estimated from the observed linewidths $\Delta B_{pp}^{\text{exp}}$ at low microwave frequencies. Such a simple convolution seems to describe simultaneously all linewidths and line shapes obtained. However, particularly the third component lacks a microscopic interpretation, and will therefore be discussed in detail in the following sections.

First, a limit will be defined in Sec. IV B for the number of interacting spins at a given ^{73}Ge concentration, for which EDMR spectra with a resolved envelope of such a hyperfine structure could be expected. Although this limit is based on a hypothetical example, it agrees fairly well with the more realistic numerical calculations presented in Sec. IV D. Close to this limit, the well known analytical models of line broadening summarized in Sec. IV C are known to be unreliable, which are the method of moments for a convolution of many discrete hyperfine constants A_n , and statistical theory for a continuous distribution function of hyperfine constants $A(r)$. Therefore, in Sec. IV D the spin localization radius r_0 is obtained by comparing $\Delta B_{pp}^{\text{conv}}$ to numerical calculations.

B. Convolution of hyperfine interactions with many nuclear spins

The large broadening without resolved substructure observed at 0.434 GHz even at the natural ^{73}Ge concentration can only be explained by hyperfine interactions with a large number of Ge nuclei. At defect concentrations around 10^{19} cm^{-3} , the large majority of atoms around the defect atom are fourfold coordinated with a hybridization close to sp^3 , so that $\alpha_n^2 \approx \frac{1}{3} \beta_n^2$ and $A_{n,\text{iso}} \gg A_{n,\text{aniso}}$, since it is known from the atomic interactions that $A_{\psi_s} \gg A_{\psi_p}$. In a disordered material, the average over many sets of hyperfine constants must be calculated for a quantitative description of the observed EDMR spectra, as the orientation and the microscopic wave function are expected to vary from one defect site to another. Methods have been developed to account for many dipolar hyperfine interactions analytically. However, in particular for the present problem of a dominant Fermi contact interaction, the analytical approaches are not applicable for the complete range of nuclear spin concentrations. Although all approaches yield very similar results in the low concentration limit and for concentrations close to $c=1$, they disagree depending on the underlying assumptions in the regime of intermediate concentrations.⁴¹

The basic convolution problem is illustrated with the help of the very simple example shown in Fig. 11. For clarity, only a single hyperfine splitting $A_n = 29 \text{ G} \times g \mu_B$ has been considered here at a nuclear spin concentration of $c=50\%$. According to Eq. (4), the pattern produced by hyperfine interaction with one single Ge nucleus consists of $2I+1$ equidistant satellites if this nucleus happens to be a ^{73}Ge atom with a nuclear spin, and of a central resonance otherwise [see Fig. 11(a)]. This corresponds to the situation of a very localized dangling bond wave function interacting only with a single nucleus. Figures 11(b) and 11(c) show the result of a threefold and tenfold convolution of this pattern with itself, which would be caused by the spread of the dangling bond wave function over three or ten nuclei with the same hypo-

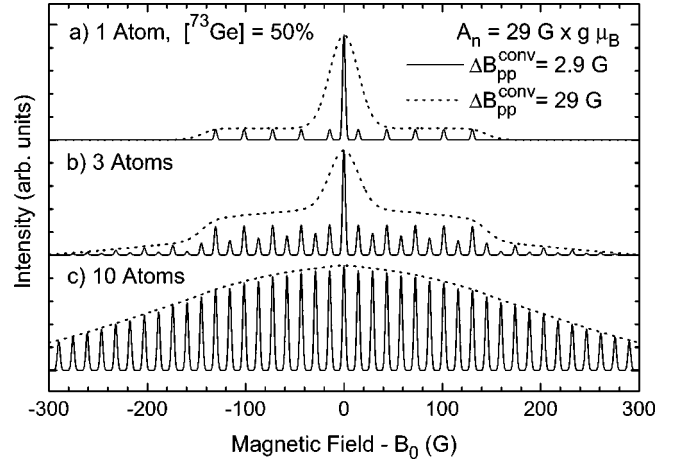


FIG. 11. Hyperfine patterns of an electronic spin with 1, 3, or 10 atoms with a probability of $c=50\%$ to have $I=9/2$ and $A_n=29 \text{ G} \times g \mu_B$. All patterns have been normalized to the maximum intensity. The spectra have been calculated with two different Gaussian lineshapes with $\Delta B_{pp}^{\text{conv}} \times g \mu_B / A_n = 0.1$ and 1. Even without any resolved hyperfine lines ($\Delta B_{pp}^{\text{conv}} = 29 \text{ G}$), the shoulders resulting from the interaction with a single ^{73}Ge spin are visible if only a small number of nuclei with a hyperfine interaction $A_n/g \mu_B \approx \Delta B_{pp}^{\text{conv}}$ are participating in the hyperfine interaction.

thetical hyperfine interaction $A_n = 29 \text{ G} \times g \mu_B$. The intensity of the hyperfine satellites for these patterns increases as the probability of finding at least one nuclear spin increases with the number of nuclei involved. As the probability of interactions with multiple nuclear spins is shared among a large number of satellites at $I=9/2$, their individual intensity is still lower than the central resonance up to rather high ^{73}Ge concentrations. The individual satellites are completely resolved in the example of Fig. 11 with an additional Gaussian broadening of $\Delta B_{pp}^{\text{conv}} = 0.1 \times A_n / g \mu_B$. However, they are smeared out with $\Delta B_{pp}^{\text{conv}} = A_n / g \mu_B$. The reason of such a broadening could, e.g., originate from a different set of nuclear spins with a smaller unresolved hyperfine splitting. Note that a different pattern would arise from fluctuations of the hyperfine constant A_n itself, which would dominantly broaden the outer hyperfine satellites. As shown in Fig. 11, the envelope structure of the satellite groups can still be resolved even if the individual broadenings $\Delta B_{pp}^{\text{conv}}$ are larger than the hyperfine splitting A_n . Approximately Gaussian line shapes are obtained only with a large enough value $N \times c$ for the number of nuclei contributing with one nuclear spin.

A quantitative criterion for the number of Ge nuclei participating in a spectrum without resolved satellites, but with a structured envelope function can be estimated from the relative intensities of the narrow central line and the broad structures in Fig. 11. In the case of interaction with a single nucleus only [Fig. 11(a)], the area under the central resonance is proportional to the fraction $1-c$. Therefore its intensity is proportional to $(1-c)/\Delta B_{pp}^{\text{conv}}$, if all lines are convoluted with the same broadening function of width $\Delta B_{pp}^{\text{conv}}$. No resolved hyperfine satellites are expected for $\Delta B_{pp}^{\text{conv}} \geq A_n$. In this case, the shape of the envelope function depends on the broadening function only in the wings. It is flat

in the central region, as all hyperfine satellites occur with the same probability for hyperfine interactions with a single ^{73}Ge nucleus only. The area of this structure is proportional to the fraction c of interacting ^{73}Ge nuclear spins, so that its intensity is proportional to $c/[2I(A_n/g\mu_B) + \Delta B_{pp}^{\text{conv}}]$. The shape of the satellite intensity pattern is different for each number of interacting nuclei, e.g., rectangular for a single nucleus, triangular for two, and of Gaussian shape for many nuclei. Up to high ^{73}Ge concentrations, the contribution of configurations with more than one ^{73}Ge nucleus is small compared to the rectangular pattern formed by the interaction with only one nuclear spin because of the larger number of satellites. This can be seen in Fig. 11(b), where a similar shape is found for the broadened envelope function of three nuclei compared to the case of only one nucleus even at $c = 50\%$. The probability is $Nc(1-c)^{N-1}$ for finding exactly one nuclear spin out of N nuclei, which could interact with the dangling bond wave function. Therefore, the intensity of the rectangular structure caused by interactions with one nuclear spin is now increased to $I_1 \approx Nc(1-c)^{N-1}/[2I(A_n/g\mu_B) + \Delta B_{pp}^{\text{conv}}]$. At the same time, the intensity of the central line is reduced to $I_0 \approx (1-c)^N/\Delta B_{pp}^{\text{conv}}$. Neglecting the rounding effects on the spectrum by multiple interactions I_2, I_3, \dots , with several nuclear spins, which become important at larger ^{73}Ge concentrations only, the ratio of intensities $I_0/I_1 \approx 1$ defines a critical number N_c of interacting nuclei, below which a resolved wing structure and above which a Gaussian line shape is expected

$$N_c = \left[\frac{2I(A_n/g\mu_B)}{\Delta B_{pp}^{\text{conv}}} + 1 \right] \frac{1-c}{c}. \quad (7)$$

For a given number of atoms, one could similarly define a critical nuclear spin concentration, above which no resolved wings are observed. This criterion provides an estimate for the number of interacting nuclei responsible for a significant broadening at a given concentration c . Although it is based on very simple considerations, it agrees very well with the results from the numerical line shape simulations discussed below. This critical number is around 10 for $\Delta B_{pp}^{\text{conv}} \approx A_n/g\mu_B$ and $c = 50\%$, while a structureless Gaussian shape at ^{73}Ge concentrations of $c = 10\%$ would require more than 90 nuclei with similar hyperfine interactions. For ^{29}Si nuclei with the smaller nuclear spin $I_{29} = 1/2$, only one third of these nuclei would be sufficient to lead to a Gaussian line at the same nuclear spin concentration. The criterion of Eq. (7) is similarly valid for the derivative lines observed in ESR experiments, which particularly emphasize the slopes at the edges of the central line and of the flat region of the hyperfine satellites.

C. Analytical line shape calculations

Analytical expressions for the second moment M_2 and some higher moments $M_n = \int y(B)B^n dB / \int y(B)dB$ of the line shape functions $y(B)$ have been calculated for the full range of nuclear spin concentrations for the case of dipolar hyperfine interactions $A_n(\theta)$.^{20,42–46} Because second mo-

ments add up linearly for convolutions of symmetrical lines, the second moment of any resonance pattern resulting from the interaction with a series of nuclei with $I = 9/2$, concentration c , and arbitrary hyperfine interactions A_n is given by

$$M_2(c) = c \frac{33}{4} \sum_n \left(\frac{A_n}{g\mu_B} \right)^2. \quad (8)$$

For the dipolar interactions between pointlike magnetic moments in a regular lattice, the rapidly decreasing $A_{n,\text{anis}} \propto (1 - 3 \cos^2 \theta_n) r_n^{-3}$ let the sums converge despite the increasing number $N(r_n) \propto r_n^3$ of interacting spins within a sphere of increasing radius r_n . Therefore, $M_2 \propto c$ over the whole range of concentrations. For a purely Gaussian line shape, the second moment can be compared directly to the experimentally observed linewidth, as $\Delta B_{pp}^{\text{Gauss}} \propto \sqrt{M_2}$ and therefore $\Delta B_{pp}^{\text{Gauss}} \propto \sqrt{c}$. For other line shapes, the higher moments must be calculated, as they influence significantly the observable peak-to-peak linewidth $\Delta B_{pp}^{\text{exp}} \approx \pi/3 \sqrt{M_2^3/M_4}$.²¹ For example, the moments of a Lorentzian line diverge, and become finite only after an arbitrary cutoff, which removes the divergence²¹ and leads to $\Delta B_{pp}^{\text{Lorentz}} \propto M_2$ and to $\Delta B_{pp}^{\text{Lorentz}} \propto c$.

It has been shown from the analysis of dipolar interactions between identical $I = 1/2$ nuclear spins in a cubic lattice, that in such a system approximately Gaussian line shapes are expected for $c > 0.1$, because in this regime $M_4 \propto c^2$. For $c < 0.01$, however, Lorentzian line shapes are expected,⁴³ as in this regime $M_4 \propto c$. The empirical deconvolution of the experimental data shown in Fig. 10 is only possible with a broadening component $\Delta B_{pp}^{\text{conv}} \propto c$, corresponding to a Lorentzian lineshape, at least up to $c = 51\%$. The line shape factors of the experimental EDMR spectra given in Table I also show that in the intermediate range of concentrations from 7.8 to 51%, where a linear increase of the frequency-independent linewidth is observed, the EDMR lines are nearly Lorentzian. Such a hyperfine broadening is in agreement with Eq. (8), however, it requires the low concentration limit to be extended over a much larger concentration range in *a*-Ge compared to the calculations of Ref. 43 for $I = 1/2$ nuclear spins in a regular lattice. This can be understood with the help of Eq. (7), taking into account the higher nuclear spin $I_{73} = 9/2$ and a smaller number N_c of effectively similar hyperfine constants in *a*-Ge. Smaller effective values of N_c are expected for *a*-Ge because of structural disorder, and because the hyperfine interactions of the dangling bond wave function probably fall off exponentially at large distances $r(n)$, i.e., faster than the long-range dipolar interactions.

It has been discussed previously by other groups that the few nearest neighbor spins are over-weighted in a linewidth calculation based on the method of moments, as the (rare) cases of nearest neighbors with nuclear spin contribute rather strongly to all finite moments. If the wings of the resonance lines cannot be measured with sufficient accuracy, the results from the method of moments can therefore be misleading.^{45,47} In this case, the statistical theory discussed in Refs. 21, 44–47 provides a very powerful alternative to

obtain the Fourier-transformed line shape. This method is well suited for the continuum approximation required in an amorphous network and becomes particularly simple in the low concentration limit, where a Lorentzian line shape is obtained. At high nuclear spin concentrations, however, correlations in the occupation of the hypothetical continuum of possible nuclear positions become inevitable, in particular for the volume around several central atoms.⁴⁸ Few atoms with almost discrete hyperfine constants are expected to dominate the linewidth in this regime. As these are problematic to describe via the statistical theory, numerical simulations will be considered instead in the following section.

D. Numerical line shape simulation

To make predictions for the hyperfine broadening over the full concentration range, many hyperfine patterns similar to those of Fig. 11, but with different hyperfine constants have been convoluted numerically via the fast Fourier transform algorithm. We start with the description of a simple numerical example without anisotropic contributions of the hyperfine interaction ($\beta_n^2=0$) and without fluctuations of α_n^2 to avoid the averaging process over many random configurations. For the wave function amplitudes at the nuclear spin sites r_n , a hydrogenic envelope function

$$\Psi_{db}(r_n) \propto e^{-r_n/r_0} \quad (9)$$

is used, which according to Eqs. (5) and (6) leads to

$$A_{n,iso}(r_n) \propto \alpha_n^2 \Psi_{db}^2(r_n) \propto e^{-2r_n/r_0}. \quad (10)$$

This kind of wave function is commonly assumed for the description of the delocalization of DB's in transport experiments, however, it is a very crude assumption compared to the set of hyperfine constants calculated for the P_b center in Ref. 3. It is not thought to be a realistic description of a true dangling bond wave function, but it is very helpful to understand the limits to which information can be extracted from the experimental data.

To define a set of hyperfine constants A_n via Eq. (10), the positions \vec{r}_n of the host atoms need to be modeled in addition to the shape of the dangling bond wave function. The probability of finding a Ge atom at a certain distance r from a central Ge atom is given by the radial distribution function (RDF) $D(r)$, which has been determined from x-ray or electron diffraction experiments. The local environment of Ge atoms consisting of the nearest neighbors and the next few shells of atoms in amorphous Ge still resembles that of crystalline Ge, however, broadened by structural disorder.⁴⁹ In particular, the maximum of the RDF around 2.44 Å in Fig. 12 can be identified with the four nearest Ge neighboring atoms, one of which is missing in the radial distribution function of DB's in a -Ge. For larger distances, $D(r)$ rapidly approaches the limit of a homogenous medium, for which $D(r)=4\pi r^2 \varrho$ with the macroscopic atom density ϱ of a -Ge, which is similar to that of crystalline Ge ($\varrho=0.0442 \text{ \AA}^{-3}$). Figure 12 illustrates how a set of discrete nuclear positions r_n were chosen for the first numerical example discussed here. A new Ge atom with index n is placed

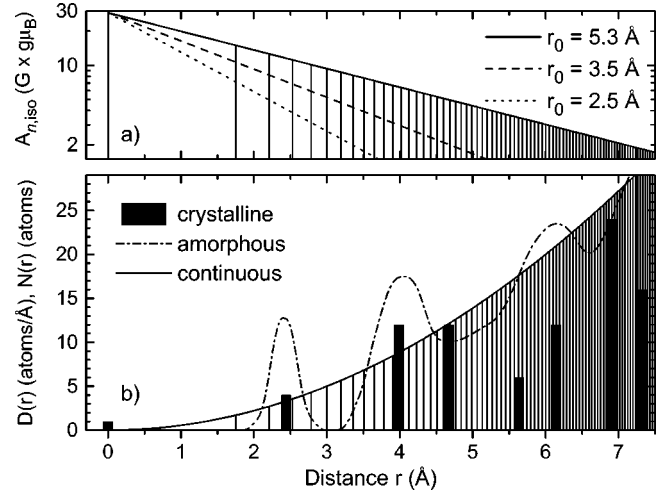


FIG. 12. (b) Radial distribution functions of crystalline Germanium [$N(r)$, bars], of a -Ge [$D(r)$, dash-dotted line, after Ref. 49], and of a homogenous medium with $D(r)=4\pi r^2 \varrho$ (solid line). The discrete atomic positions $r_n = \sqrt[3]{3n/(4\pi\varrho)}$ are chosen from $D(r)$ for a homogeneous medium such that the area below each of the resulting segments corresponds to a single atom. (a) Set of hyperfine constants $A_{n,iso}$ resulting from Fermi contact interaction of the dangling bond wave function of Eq. (9) with different localization radii r_0 .

at each distance r_n , at which the area under the continuous distribution function $\int D(r) dr = 4/3\pi r^3 \varrho = n$ corresponds to a full atom, i.e.,

$$r_n = \sqrt[3]{3n/(4\pi\varrho)}, \quad n=0,1,\dots \quad (11)$$

This ensures that at large distances the macroscopic atomic density $\varrho \approx 0.0442 \text{ \AA}^{-3}$ is obtained. In this approximation, the nearest-neighbor positions are distributed between 1.8–2.8 Å, which is a significantly larger spread than of 2.2–2.7 Å in the RDF of a -Ge. However, the results from simulations based on Eq. (11) were virtually the same as those from simulations with $r_{1-3}=2.44 \text{ \AA}$. The errors introduced by the actual choice of r_n are therefore negligible, in particular compared to the effects of spin polarization discussed in Sec. V A. The resulting hyperfine constants from Eqs. (11) and (10) are shown in Fig. 12(a) for three different localization radii and $A_0=29 \text{ G} \times g \mu_B$. Note that for a spin density of DB's of about 10^{19} cm^{-3} , each defect occupies the volume of a sphere with a radius of $20 \text{ \AA} \gg r_0$. The sum of the different sets of hyperfine constants of Fig. 12(a) is of interest for the normalization condition $\sum_n \alpha_n^2 + \beta_n^2 = 1$ of the dangling bond wave function. It is about 190 G for the set of hyperfine constants with $r_0=3.5 \text{ \AA}$, and about 85 and 620 G for those with $r_0=2.5$ and 5.3 \AA , respectively.

The derivative spectra, which result from the convolution of the hyperfine patterns obtained for the three sets of hyperfine constants of Fig. 12(a) are shown in Fig. 13. Whereas the second moments of the simulated spectra fulfill Eq. (8) for all concentrations, their line shapes are obviously different than both Gaussian and Lorentzian curves. The overall shape of the simulated spectra is more similar to a Lorentzian curve up to $c=60\%$, and to a Gaussian curve for higher

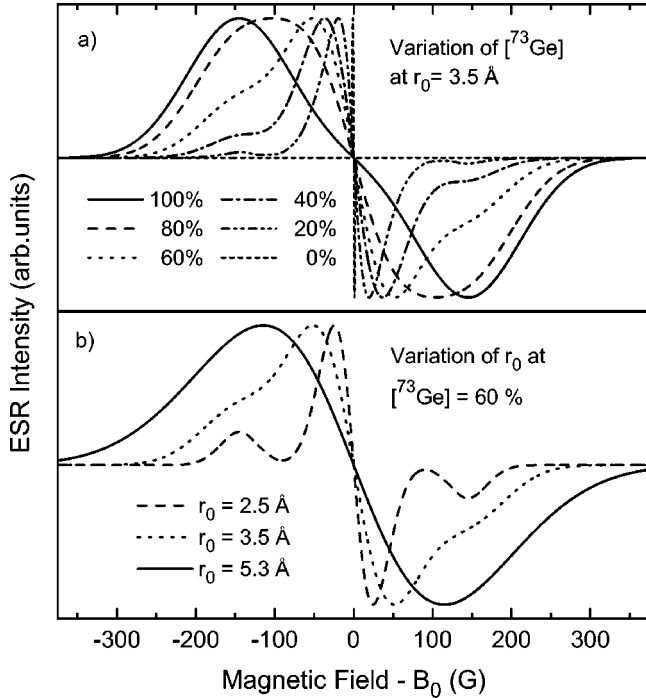


FIG. 13. (a) Simulated spin resonance spectra for the model of Fig. 12 for a localization radius of $r_0 = 3.5 \text{ \AA}$. The resolved shoulders originate from the hyperfine interaction $A_{0,\text{iso}} = 29 \text{ G} \times g \mu_B$ with the central ^{73}Ge defect atom. In the experimental spectra, these shoulders are averaged out because of fluctuations of the hyperfine constants, e.g., due to a dipolar hyperfine interaction $A_{0,\text{aniso}} \geq 5 \text{ G} \times g \mu_B$ at the same defect atom. Part (b) shows the simulated spectra obtained for $r_0 = 2.5, 3.5,$ and 5.3 \AA at $c = 60\%$.

c. A shoulder structure similar to that found in Fig. 11 and at the position of the experimentally observed wings of Fig. 8 is resolved at low concentrations. Obviously, the assumed hyperfine interaction $A_{0,\text{iso}} = 29 \text{ G} \times g \mu_B$ of the central ^{73}Ge defect atom differs enough from $A_{n \geq 1} < 11 \text{ G} \times g \mu_B$ assumed for the backbonding neighbors, so that in this model the shoulders of Fig. 11 remain visible.

The peak-to-peak linewidth $\Delta B_{pp}^{\text{num}}$ of the simulated derivative spectra can be determined numerically from the magnetic field separation of its global maximum and minimum. The theoretical linewidths obtained via this method for the three different radii of localization are shown in Fig. 14, with the linewidths corresponding to $r_0 = 3.5 \text{ \AA}$ in Fig. 14(b). An increase of the linewidth approximately linear with the ^{73}Ge concentration is observed up to $c = 60\%$ for $r_0 = 3.5 \text{ \AA}$. Above $c = 80\%$, the linewidth rapidly approaches $\Delta B_{pp}^{\text{num}} \approx 300 \text{ G}$. The resulting step of the linewidth around $c = 80\%$ is related to the cross-over between the central line of this pattern from DB's centered at nuclei with $I = 0$ and the $2I + 1$ equally intense contributions of hyperfine satellites already discussed in the context of Fig. 10.

This step is not present assuming a larger $r_0 = 5.3 \text{ \AA}$ [Fig. 14(a)]. In that case, the linewidth of the spectrum at $c = 60\%$ shown in Fig. 13(b) is large enough to cover the satellite pattern of the central atom, mainly because of the smaller difference between the largest hyperfine constant $A_0 = 29 \text{ G} \times g \mu_B$ of the central atom and $A_1 \approx 15 \text{ G} \times g \mu_B$

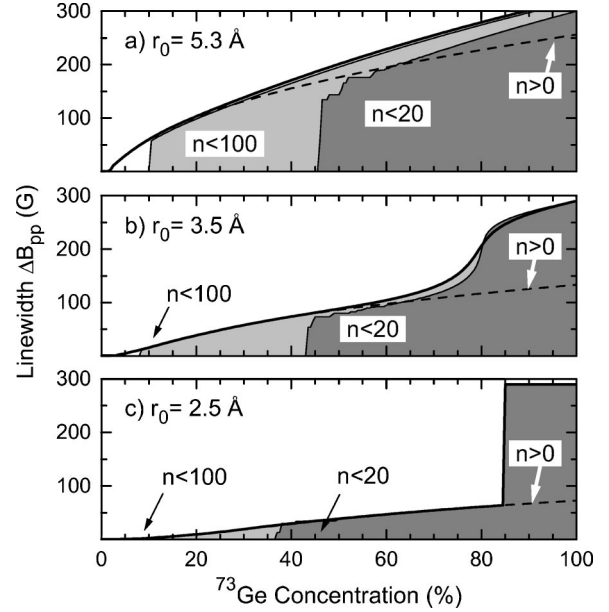


FIG. 14. Peak-to-peak linewidth $\Delta B_{pp}^{\text{num}}$ extracted from the maximum and minimum field positions of the spectra obtained for the three sets of hyperfine constants of Fig. 12(a). The satellite structures causing the step around 80% in the linewidth at localization radii of (c) $r_0 = 2.5$ and (b) $r_0 = 3.5 \text{ \AA}$ vanish at a localization radius of (a) $r_0 = 5.3 \text{ \AA}$ because of the larger number of similar hyperfine constants. The dashed line was simulated without a central atom ($n > 0$), and the shaded areas indicate the linewidths calculated for the hyperfine constants with the nearest $n < 20$, and $n < 100$ nuclei.

attributed to one of the backbonding neighbors in this model. As the linewidth of the central line for $r_0 = 5.3 \text{ \AA}$ is around 200 G at $c = 60\%$, the satellites collapse with the central line for the solid curve in Fig. 13(b). Because an accumulation of sufficient nuclei with similar hyperfine constants occurs for this localization radius according to Eq. (7) already for concentrations above 5% , the line shapes are rather Gaussian, as shown in Fig. 15(a), where the line shape factor l determined numerically from the simulated spectra is plotted with solid lines for the same model used in Figs. 13 and 14. As expected for a Gaussian line shape, $\Delta B_{pp}^{\text{num}} \propto \sqrt{c}$ is found over almost the entire concentration range [see Fig. 14(a)].

In contrast, the satellite structure is clearly resolved for spectra simulated with a shorter localization radius $r_0 = 2.5 \text{ \AA}$. In this case, a central line is resolved between two distinct satellite peaks, which makes the definition of a single linewidth $\Delta B_{pp}^{\text{num}}$ difficult. Consequently, a jump of the linewidth occurs again, when the intensity of the outer satellites becomes larger than the intensity of the central line. At sufficiently low concentrations, the linewidth increases almost linearly with the ^{73}Ge concentration, as appropriate for a Lorentzian line shape. The line shape factors obtained numerically for these spectra are shown in Fig. 15(c) and are close to the Lorentzian value in the intermediate concentration range. They can be compared better with the experimental values of Table I, if the additional broadening mechanisms at the different microwave frequencies are taken into account. The dominant mechanism at 9.35 GHz is g -factor

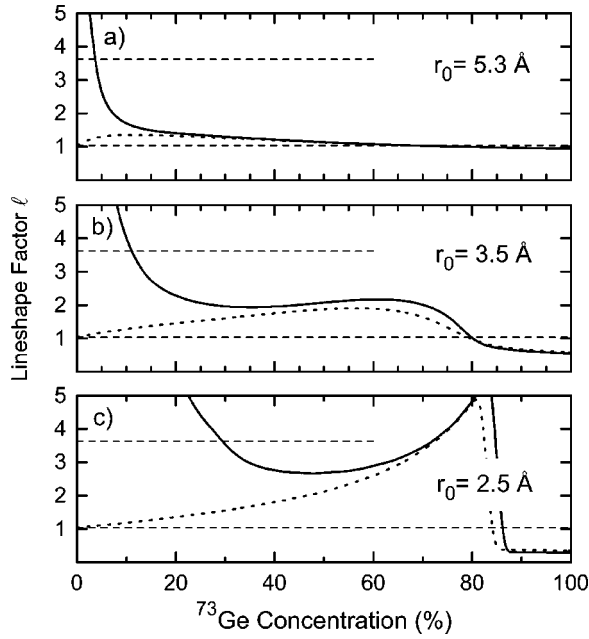


FIG. 15. The line shape factors l determined from the calculated spectra for the three sets of hyperfine constants of Fig. 12(a) (full lines). For a localization radius $r_0 = 5.3$ Å, l is close to the Gaussian value of 1.033. For smaller r_0 , a Gaussian line is only expected for large ^{73}Ge concentrations. In the intermediate concentration range, l is closer to 3.628, which would be expected for a purely Lorentzian line. Also included are the lineshape factors expected for the three cases when Gaussian g -factor broadening $\Delta B_{pp}^{\text{SO}} \approx 40$ G at 9.35 GHz is included (dotted lines).

broadening, as discussed in Sec. III A with $\Delta B_{pp}^{\text{SO}} \approx 40$ G and an approximately Gaussian shape. The line shape factors of the numerical spectra with such an additional broadening are shown by the dotted lines in Fig. 15. In agreement with the experimental data, the line shapes start from a Gaussian shape at low nuclear spin concentrations, where g -factor broadening dominates, become Lorentzian at intermediate concentrations, and Gaussian again at $c > 80\%$.

The validity of Eq. (7) not only for one fixed hyperfine constant, but also for the sets of hyperfine constants discussed here, is shown numerically in Fig. 14 for a partial convolution of the hyperfine patterns of the nearest 20 or 100 neighboring nuclei only, and for the convolution of the complete set without the central defect atom. The steplike structure above $c = 80\%$ can be attributed unambiguously to the central atom, as it is not observed if the central atom is removed from the convolution. As seen by the steps in the curves with $n \leq 20$ and 100 atoms, the simulated linewidth is dominated by interactions with the central 20 nuclei for $c \geq 40\%$ and with the central 100 nuclei at $c \geq 10\%$. Both numbers are in good agreement with Eq. (7) for $\Delta B_{pp}^{\text{conv}} \approx 2I(A_n/g\mu_B)$.

Obviously, most of the information on individual hyperfine constants is lost during the convolution process. It is therefore not surprising that similar line shapes and linewidths can be obtained numerically not only for the specific set of hyperfine constants shown in Fig. 12(a), but also for other wave function envelopes with similar localization

lengths and for other radial distribution functions consistent with the macroscopic density of a -Ge. A quasi-continuous RDF can be modeled numerically, e.g., with a large number of DB's, each with its characteristic distribution function of atomic distances r_n and hyperfine constants A_n . The average ESR spectra for these DB's, and the corresponding linewidths and line shapes are not much different from the results of Figs. 14 and 15. Independent of the specific defect model, the approximately Lorentzian line shape and $\Delta B_{pp}^{\text{num}} \propto c$ up to $c = 60\%$, as well as the sudden increase to a linewidth of about 300 G are typical for those sets of hyperfine constants with $A_{0,\text{iso}} = 29 \text{ G} \times g\mu_B$ and a localization parameter around 3.5 Å. The available experimental data points, which indicate a hyperfine broadening of 10 G at $c = 7.8\%$, of 70 G at $c = 51\%$, and of 300 G at $c = 95.6\%$ could be reproduced by those defect models containing 1–2 atoms with $A_n \approx 29 \text{ G} \times g\mu_B$, 3–6 atoms with $A_n \approx 4 - 10 \text{ G} \times g\mu_B$, and 100–200 atoms with $A_n \approx 0.5 - 1 \text{ G} \times g\mu_B$, irrespective of the exact distribution functions. Within the given ranges, the larger number of nuclei is always to be used in conjunction with the smaller hyperfine constant. The ranges of validity were obtained by numerical simulations, but could have been determined as well with the numbers of nuclei from Eq. (7) for a given concentration and a typical set of hyperfine constants, and the linewidths from the ratio of the cumulated moments M_2 and M_4 .

The sum of all isotropic hyperfine interactions with the dangling bond wavefunction is in the range of 160–190 G for those sets of hyperfine constants, which are consistent with the experimental data. Also for the model of Fig. 12 this sum is about 190 G at a localization radius of 3.5 Å. Compared to the tabulated atomic hyperfine interaction of $843 \text{ G} \times g_0\mu_B$ for an ideal $4s$ orbital, this suggests that about 19–23% of the dangling bond wave function occupies s -like atomic orbitals. Only 3.4% of an atomic s -wave function is found at the central Ge atom. The non- s -like 77–81% of the wave function are expected to occupy p -like atomic orbitals, probably with an s/p ratio significantly smaller than 1/3 at the central atom and significantly larger at remote atoms. Note that the sums of the isotropic hyperfine constants of Fig. 12 for $r_0 \approx 2.5$ and 5.3 Å of 85 and 620 $\text{G} \times g\mu_B$ would be unrealistic, so that all $A_{n,\text{iso}}$ would need to be scaled up or down for these cases by a factor of 2–4 to fulfill the normalization condition. Then, however, the linewidth at $c = 100\%$ would be far from the experimentally observed values.

Until now, we have not taken into account any contributions of $A_{n,\text{aniso}}$. Because all orientations of DB's are distributed randomly in amorphous materials, this will lead to powder pattern distributions of hyperfine constants between $A_{n,\perp} = A_{n,\text{iso}} - A_{n,\text{aniso}}$ and $A_{n,\parallel} = A_{n,\text{iso}} + 2A_{n,\text{aniso}}$ in addition to the random fluctuations of $A_{n,\text{iso}}$ due to disorder. Such fluctuations of $A_{0,\text{iso}}$ are required to account for the observation of a structureless spectrum, even if $\Delta B_{pp}^{\text{exp}} \ll A_{0,\text{iso}}$, which is the case at 0.434 and 2.00 GHz and $c = 7.8\%$. Without such fluctuations, the simulations of Fig. 13(a) show a local minimum around $B_0 \pm 120$ G and a maximum around $B_0 \pm 150$ G. These features would overlap, if their position fluctuated by about 30 G, i.e., with fluctuations of A_n of at

least 20% or $6 \text{ G} \times g\mu_B$. Because of the sharp peak of the powder pattern distribution at $A_{0,\perp}$, the interpretation of these fluctuations as anisotropic hyperfine interaction would require even larger fluctuations of $A_{0,\text{aniso}} \geq 5 \text{ G} \times g\mu_B$ in order to average out the wings of the spectra shown in Fig. 13(a) according to numerical simulations including $A_{0,\text{aniso}}$. For very large values of $A_{0,\text{aniso}}$, the true value of $A_{0,\text{iso}}$ would be somewhat higher than $29 \text{ G} \times g\mu_B$ because of the asymmetry of the hyperfine powder patterns.

To summarize the results of the numerical simulations, the experimental linewidths and line shapes can be explained by a dangling bond model wave function with $A_{0,\text{iso}} = 29 \text{ G} \times g\mu_B$ and a radius of localization $r_0 = 3.5 \text{ \AA}$, irrespective of the particular model employed. In agreement with the simple estimate from Eq. (7), at least 20 central nuclei are found to contribute to the linewidth at $c \approx 40\%$, and at least 100 central nuclei to the linewidth at $c \approx 10\%$. More complicated statistical models with fluctuating hyperfine constants or $A_{0,\text{aniso}} \geq 5 \text{ G} \times g\mu_B$ are required to account for the structureless wings of the experimental spectra.

V. DISCUSSION

Based on the conclusions for the hyperfine parameters of DB's in *a*-Ge, the microscopic structure suggested from this work for DB's in *a*-Ge will be discussed in Sec. V A taking into account the effects of spin polarization. The considered defect structure is then compared to the localization radius obtained from transport experiments and to the structure of DB's in *a*-Si:H in Sec. V B.

A. Spin polarization

According to Eq. (5), the hyperfine parameters $A_{n,\text{iso}}$ and $A_{n,\text{aniso}}$ are usually evaluated in terms of the fractions α_n and β_n of *s*- and *p*-like atomic orbitals contributing to the full dangling bond wave function. The corresponding spin densities α_n^2 and β_n^2 are obtained via Eq. (6) by comparison of the experimental parameters with the atomic values from Hartree-Fock calculations. Accordingly, $A_{0,\text{iso}} = 29 \text{ G} \times g\mu_B$ corresponds to an *s*-like contribution of $\alpha_0^2 = 3.4\%$ at the central atom.

$A_{0,\text{aniso}} \geq 5 \text{ G}$ can only be estimated roughly from the missing structure of the experimental spectra at $c = 7.8\%$, which requires a certain random variation of A_0 . If these variations were dominated by anisotropic hyperfine interaction, the *p*-wave fraction at the central atom would be $\beta_0^2 \geq 30\%$, and the *s/p* hybridization ratio at the central defect atom $\alpha_0^2/\beta_0^2 \leq 11\%$, as compared to the ratio of about 12% determined from $\alpha_0^2 = 6\%$ and $\beta_0^2 \approx 50\%$ for DB's in *a*-Si:H in Refs. 8,9. For SiH_3 and GeH_3 radicals with negligible delocalization and small spin polarization of the bonds, the *s* character at the defect atom was evaluated to be around 21 and 11.5%, respectively.^{50,51} As the value for GeH_3 is based on the rather small atomic Fermi contact interaction of $A_{\Psi_s} = 535 \text{ G} \times g_0\mu_B$ from Ref. 18, even smaller fractions α_0^2/β_0^2 around 7% would be obtained for DB's in GeH_3 radicals based on the more recent value $A_{\Psi_s} = 843 \text{ G} \times g_0\mu_B$ of Ref.

17 used here. Therefore, the hybridization ratio at the Ge atom in GeH_3 is probably even lower, indicating nearly complete *sp*² configuration of the Ge-H bonds and a significant relaxation of the defect atom into the plane of the backbonding H atoms. Taking into account the smaller *s/p* ratio of DB's in *a*-Si:H with respect to the SiH_3 radical, one could expect a hybridization ratio even below 7% for DB's in *a*-Ge, resulting in $\beta_0^2 \geq 50\%$ and $A_{0,\text{aniso}} \geq 9 \text{ G}$.

However, as indicated by the localization radius for $A_{n,\text{iso}}$ in Sec. IV D, large parts of the dangling bond wave function in *a*-Ge seem not to be located on the dangling bond defect atom itself. For these sets of hyperfine constants compatible with the experimental data in Sec. IV D, the sum of the isotropic hyperfine interactions with remote nuclei $\sum_{n \geq 1} A_{n,\text{iso}}$ is typically around 130–160 $\text{G} \times g\mu_B$, suggesting that about 15–19% of the dangling bond wave function occupies *s*-like states at Ge atoms other than the central defect atom. Assuming a hybridization ratio $s/p \approx 1/3$ (*sp*³ configuration) for these remote atoms, this would correspond to 60–76% of the complete defect wave function. The sum of the three contributions $\alpha_0^2 = 3.4\%$, $\beta_0^2 \geq 50\%$, and $\sum_{n \geq 1} 4\alpha_n^2 = 60\text{--}76\%$ is somewhat larger than 100%, but at least of the correct order of magnitude. The difference could indicate a lower *p* fraction than $s/p \approx 1/3$ at the remote atoms, or, alternatively, some of the atomic spin densities α_n^2 to be negative, which could not be distinguished in the experimental broadenings discussed above.

Negative spin densities are only one consequence of spin-polarization effects, which are well known for DB's in *a*-Si:H. Although the model wave function of Eq. (5) provides a reasonable approximation for the dangling bond charge density, the same wave function is probably inappropriate to give a realistic description of the dangling bond spin densities. Hartree-Fock calculations for the atomic hyperfine constants include the contributions from core polarization as a spin-dependent deformation of the Ge inner *1s*-*3s* shells, described by configuration interactions.¹⁸ As is known from the hyperfine interactions in small molecules, such a core polarization strongly depends on the unpaired spin density in the valence state. In different bonding configurations, the spin polarization might vary with respect to the atomic values. A single experimental hyperfine parameter α_n^2 or β_n^2 is then insufficient to quantify these multiple effects, so that the calculated localization based on $\alpha_n^2 + \beta_n^2$ is incorrect for the charge density in most cases.³ Furthermore, even in the absence of net charge or unpaired spin density at one Ge atom, charge density on neighboring Ge atoms will cause locally unbalanced positive and negative spin densities at the central atom by local polarization of the bonds. This spin density then occurs with the opposite sign at the other atoms.

For the GeH_3 radical, this spin polarization of the bonds was measured from the proton interaction to contribute with $13 \text{ G} \times g\mu_B$ to the total isotropic hyperfine coupling of the ⁷³Ge nuclei of $75 \text{ G} \times g\mu_B$.^{50,51} Such a shift of positive spin density from the ligands to the central atom would be significant compared to $A_0 = 29 \text{ G} \times g\mu_B$ and $A_1 = 10 \text{ G} \times g\mu_B$ of the model wave function with $r_0 = 3.5 \text{ \AA}$, and hence the *s*-like charge density at the central atom is possibly even

lower than 3.4%. In *a*-Ge, the spin polarization at the central atom is probably smaller than in GeH₃ because of charge delocalization. However, as pointed out in Ref. 3, also for DB's at the Si/SiO₂ interface the spin density at the neighboring atoms is almost cancelled by the transfer of spin density towards the central atom. Spin polarization also explains the difference between the charge and spin densities calculated for DB's in *a*-Si in Ref. 13, which predict a charge localization below 20%, but a spin localization around 50% at the central atom.

Because the fraction of the dangling bond wave function is largest at the central atom, the negative contributions to the spin density are largest on the backbonding atoms. At these atoms, the balance of opposing contributions may cause a reduction of the actual hyperfine interaction to zero or below, which once more justifies the assumption of a distinct isotropic hyperfine interaction $A_{0,\text{iso}} \gg A_{n,\text{iso}}$ at the central defect atom, which is one of the characteristic results of the numerical simulations of Sec. IV D. The remote atoms, which determine the linewidth at smaller nuclear spin concentrations with their small hyperfine constants, are therefore an alternative and possibly more universal basis for the definition of a spin localization parameter of DB's in different materials, as they do not suffer such large spin polarization effects as the central defect atoms.

As a consequence of spin polarization, a spin-unrestricted wave function in contrast to Eq. (5) cannot be easily identified with the experimentally accessible hyperfine parameters. Therefore, detailed theoretical calculations are required to interpret the experimental parameters quantitatively. Such calculations could also clarify, whether the postulated fluctuations of A_0 around $A_{0,\text{iso}}$ can indeed be ascribed to anisotropic hyperfine interactions.

B. Charge localization

The low temperature transport properties of *a*-Ge are strongly influenced by the extent of the dangling bond defect wave function. The characteristic hopping rates of spin-independent transport are determined by charge, not spin localization. However, both types of wave functions must be considered in a realistic model for the dangling bond wave function, as pointed out previously for the P_b center and DB's in *a*-Si:H.^{3,13} The charge localization radius r_c of DB's in *a*-Ge:H has been determined from dc transport measurements in Ref. 14. According to the Mott model, the variable range hopping conductivity for delocalized DB's described by Eq. (9) is given by

$$\sigma \propto e^{-\eta(T/T_0)^{-1/4}}, \quad (12)$$

where $T_0^{-1} = r_c^3 N_F k_B$, and with the factor η in the range between 0.9 and 1.3, depending on the employed theoretical model. The density of states at the Fermi level N_F is linked to the spin density N_S via the density of states according to $N_F = N_S \times 11 \text{ eV}^{-1}$, which can be obtained from deep level transient spectroscopy.⁵² From Eq. (12), a localization radius of the order of 1 Å would be obtained with $T_0 = 2 \times 10^8 \text{ K}$ from the inset of Fig. 1. However, because unwanted influences of temperature cannot be excluded in measurements of

$\sigma(T)$, the determination of r_c from T_0 is regarded as being very unreliable. Therefore, the dependence of $\sigma(N_F)$ on the spin density was evaluated for *a*-Ge:H in Ref. 14 at a fixed temperature $T = 200 \text{ K}$ with spin densities of DB's in range of 10^{17} to 10^{18} cm^{-3} after electron irradiation and stepwise annealing, resulting in a charge localization radius around $r_c = 11 \text{ Å}$. The same hopping processes are also believed to be responsible for the lifetime broadening of the ESR signals at higher temperatures.^{19,28,29,33,53}

The charge localization radius $r_0 = 11 \text{ Å}$ of DB's in *a*-Ge:H is about three times larger than the spin localization radius $r_0 = 3.5 \text{ Å}$ determined from the hyperfine broadening in this work. For DB's in *a*-Si:H, a charge localization radius around 4 Å has been determined from transport experiments at 200 K in Ref. 14, while the resolved hyperfine data of the central atoms in *a*-Si:H would be consistent with a spin localization radius of 3 Å.⁷

It remains to be shown whether the localization parameters determined from the central hyperfine interactions at the few central atoms of the DB's in *a*-Si are equivalent to r_0 extracted from the more than 100 remote atoms in this work, and independent of the relaxation at the central atom. The comparison of both models is possible for DB's in *a*-Si, for which both the hyperfine interactions at the central atom as well as the hyperfine broadening at low ²⁹Si concentrations⁹ have been measured. With a model wave function for DB's in *a*-Si similar to that of Fig. 12(a), but with $I_{29} = 1/2$, $A_{0,\text{iso}} \approx 70 \text{ G} \times g \mu_B$, and $r_0 = 3.0 \text{ Å}$, hyperfine broadenings of $\Delta B_{pp}^{\text{conv}}/c \approx 40 \text{ G}$ can be predicted from numerical simulations for $c \leq 10\%$. This is in good agreement with the experimental low-frequency data of Ref. 9, which shows $\Delta B_{pp}^{\text{exp}}/c \approx 40 \text{ G}$ for isotopically diluted *a*-Si:H samples. The critical number of nuclei of Eq. (7) is lower in *a*-Si than in *a*-Ge because of the smaller nuclear spin. Therefore, and because of the smaller localization radius, the linewidth in *a*-Si is not expected to rise linearly up to 50%, but to show a second steplike structure at ²⁹Si concentrations around 20% due to the backbonding atoms. For DB's in *a*-Si, the spin localization radius derived from the central and outer atoms apparently agree in the investigated concentration range. The spin localization radius can be checked once more at the central hyperfine constant via the normalization condition for the dangling bond wave function in *a*-Ge. The volume occupied by a delocalized spin wave function scales as r_0^3 , so that the spin density at the central atom would be expected to be about $(3.5/3.0)^3 = 1.6$ times smaller for DB's in *a*-Ge compared to *a*-Si based on the localization radii, consistent with $\alpha_0^2 + \beta_0^2 \approx 50\text{--}70\%$ for *a*-Si and about 30–50%, which is most probable for *a*-Ge.

Therefore, both the broadening at low nuclear spin concentrations and the central hyperfine constants support a spin localization radius of $r_0 = 3.5 \text{ Å}$ for DB's in *a*-Ge compared to $r_0 = 3.0 \text{ Å}$ for DB's in *a*-Si. In *a*-Ge, however, this spin delocalization parameter is significantly smaller than the charge localization radius of 11 Å of Ref. 14. This shows that spin-unrestricted calculations will be indispensable to model the dangling bond wave functions in amorphous germanium.

VI. CONCLUSIONS

Broadening of the spin resonance signal of DB's in *a*-Ge from 2.6 to 300 G was observed in EDMR investigations of isotope-engineered *a*-Ge samples over the whole ^{73}Ge concentration range from 0.1 to 95.6%. The contributions of *g*-factor broadening of $\Delta B_{pp}^{\text{SO}} = 4.4 \text{ G} \times \nu/\text{GHz}$ and of dipolar broadening of the order of 1 G were investigated separately from these hyperfine contributions with the help of measurements on a nuclear-spin free *a*- ^{70}Ge sample. An additional hyperfine broadening of 10 G due to the ^{73}Ge spins is observed at the natural isotope concentration. Although no hyperfine satellites are resolved due to the continuously increasing linewidth and the large number of contributing nuclear spins, a central hyperfine interaction of

$A_{0,\text{iso}} = 29 \text{ G} \times g\mu_B$ and a spin localization radius $r_0 = 3.5 \text{ \AA}$ are extracted from numerical simulation of the ^{73}Ge concentration dependence of the spin resonance linewidth and line shape. The spin density is found to be three times more localized than the charge density at the charge localization radius of *a*-Ge determined from transport measurements.

ACKNOWLEDGMENTS

The work at Walter Schottky Institut was supported by Deutsche Forschungsgemeinschaft, and the work at Keio University in part by the Grant-in-Aid from the Ministry of Education, Sport, Science and Culture of Japan, Grant No. 14076215. The authors are thankful to E. Bauer for the experimental assistance with the 2.00 GHz microwave system.

*Electronic address: tobias.graf@wsi.tum.de

- ¹K.L. Brower, Appl. Phys. Lett. **43**, 1111 (1983).
- ²W.E. Carlos, Appl. Phys. Lett. **50**, 1450 (1987).
- ³M. Cook and C.T. White, Phys. Rev. B **38**, 9674 (1988).
- ⁴E.H. Poindexter, P.J. Caplan, B.E. Deal, and R.R. Razouk, J. Appl. Phys. **52**, 879 (1981).
- ⁵T.D. Mishima, P.M. Lenahan, and W. Weber, Appl. Phys. Lett. **76**, 3771 (2000).
- ⁶A. Stesmans and V. Afanas'ev, Phys. Rev. B **57**, 10 030 (1998).
- ⁷D. Biegelsen and M. Stutzmann, Phys. Rev. B **33**, 3006 (1986).
- ⁸M. Stutzmann and D.K. Biegelsen, Phys. Rev. B **40**, 9834 (1989).
- ⁹T. Umeda, S. Yamasaki, J. Isoya, and K. Tanaka, Phys. Rev. B **59**, 4849 (1999).
- ¹⁰H. Yokomichi, I. Hirabayashi, and K. Morigaki, Solid State Commun. **61**, 697 (1987).
- ¹¹H. Yokomichi and K. Morigaki, J. Non-Cryst. Solids **97-98**, 67 (1987).
- ¹²N. Ishii and T. Shimizu, Phys. Rev. B **42**, 9697 (1990).
- ¹³P.A. Fedders, D.A. Drabold, P. Ordejón, G. Fabricius, D. Sa'nchez-Portal, E. Artacho, and J.M. Soler, Phys. Rev. B **60**, 10 594 (1999).
- ¹⁴M. Stutzmann and J. Stuke, Solid State Commun. **47**, 635 (1983).
- ¹⁵F.C. Marques, M.M. de Lima, Jr., and P.C. Taylor, J. Non-Cryst. Solids **266-269**, 717 (2000).
- ¹⁶C.F.O. Graeff, M. Stutzmann, and M.S. Brandt, Phys. Rev. B **49**, 11 028 (1994).
- ¹⁷J. A. Weil, J. R. Bolton, and J. E. Wertz, *Electron Paramagnetic Resonance* (Wiley, New York, 1994).
- ¹⁸P. W. Atkins and M. C. R. Symonis, *The Structure of Inorganic Radicals* (Elsevier, Amsterdam, 1967).
- ¹⁹B. Movaghar, L. Schweitzer, and H. Overhof, Philos. Mag. B **37**, 683 (1978).
- ²⁰J.H.V. Vleck, Phys. Rev. **74**, 1168 (1948).
- ²¹A. Abragam and B. Bleaney, *Electron Paramagnetic Resonance of Transitions Ions* (Oxford University Press, Oxford, 1970).
- ²²R. Vrijen, E. Yablonovitch, K. Wang, H.W. Jiang, A. Balandin, V. Roychowdhury, T. Mor, and D. DiVincenzo, Phys. Rev. A **62**, 012306 (2000).
- ²³K. Itoh, W.L. Hansen, E.E. Haller, J.W. Farmer, V.I. Ozhogin, A. Rudnev, and A. Tikhomirov, J. Mater. Sci. **8**, 1341 (1993).
- ²⁴M. Stutzmann and D.K. Biegelsen, Phys. Rev. B **28**, 6256 (1983).
- ²⁵N. Kishimoto, K. Morigaki, and K. Murakami, J. Phys. Soc. Jpn. **50**, 1970 (1981).
- ²⁶M.S. Brandt and M. Stutzmann, Phys. Rev. B **43**, 5184 (1991).
- ²⁷K. Lips, S. Schütte, and W. Fuhs, Philos. Mag. B **65**, 945 (1992).
- ²⁸S. Hasegawa and S. Yazaki, Philos. Mag. B **45**, 347 (1982).
- ²⁹B. Movaghar and L. Schweitzer, Phys. Status Solidi B **80**, 491 (1977).
- ³⁰N.F. Mott and E.A. Davis, *Electronic Processes in Non-Crystalline Materials* (Clarendon Press, Oxford, 1971).
- ³¹S. Greulich-Weber, Phys. Status Solidi A **162**, 95 (1997).
- ³²R.G. Barnes and W.V. Smith, Phys. Rev. **93**, 95 (1954).
- ³³G.A.N. Connell and J.R. Pawlik, Phys. Rev. B **13**, 787 (1976).
- ³⁴L. Kuebler, G. Gewinner, J.J. Koulmann, and A. Jaéglé, Phys. Status Solidi B **78**, 149 (1976).
- ³⁵J. Stuke, Amorphous Liq. Semicond. **7**, 407 (1977).
- ³⁶S. Lebib, M. Schoisswohl, J.L. Cantin, and H.J. von Bardeleben, Thin Solid Films **294**, 242 (1997).
- ³⁷P.R. Cullis and J.R. Marko, Phys. Rev. B **11**, 4184 (1975).
- ³⁸H. Dersch, L. Schweitzer, and J. Stuke, Phys. Rev. B **28**, 4678 (1983).
- ³⁹M.S. Brandt, M.W. Bayerl, M. Stutzmann, and C.F.O. Graeff, J. Non-Cryst. Solids **227-230**, 343 (1998).
- ⁴⁰R.J. McEachern and J.A. Weil, Phys. Rev. B **49**, 6698 (1994).
- ⁴¹C.W. Myles, Phys. Rev. B **14**, 14 (1976).
- ⁴²A.F. Kip, C. Kittel, R.A. Levy, and A.M. Portis, Phys. Rev. **91**, 1066 (1953).
- ⁴³C. Kittel and E. Abrahams, Phys. Rev. **90**, 238 (1953).
- ⁴⁴M.H. Cohen and F. Reif, Solid State Phys. **5**, 321 (1957).
- ⁴⁵A.M. Stoneham, Rev. Mod. Phys. **41**, 82 (1969).
- ⁴⁶D.K. Wilson, Phys. Rev. **134**, A265 (1964).
- ⁴⁷P.A. Fedders, Phys. Rev. B **11**, 1020 (1975).
- ⁴⁸D. Freude and H. Schmiedel, Phys. Status Solidi B **54**, 631 (1972).
- ⁴⁹M. Stutzmann, *Amorphous Semiconductors*, Vol. 3 of *Handbook on Semiconductors*, edited by T. S. Moss (Elsevier Science, B.V., 1994), p. 657.
- ⁵⁰G.S. Jackel, J.J. Christiansen, and W. Gordy, J. Chem. Phys. **47**, 4274 (1967).
- ⁵¹G.S. Jackel and W. Gordy, J. Chem. Phys. **47**, 4274 (1967).
- ⁵²J.D. Cohen, J.P. Harbison, and K.W. Wecht, Phys. Rev. Lett. **48**, 109 (1982).
- ⁵³S. Hasegawa and Y. Imai, Philos. Mag. B **45**, 347 (1982).